

Lattice Boltzmann modeling of transport phenomena in fuel cells and flow batteries

Ao Xu¹ · Wei Shyy¹ · Tianshou Zhao¹

Received: 6 February 2017 / Accepted: 14 March 2017 / Published online: 28 April 2017

© The Chinese Society of Theoretical and Applied Mechanics; Institute of Mechanics, Chinese Academy of Sciences and Springer-Verlag Berlin Heidelberg 2017

Abstract Fuel cells and flow batteries are promising technologies to address climate change and air pollution problems. An understanding of the complex multiscale and multiphysics transport phenomena occurring in these electrochemical systems requires powerful numerical tools. Over the past decades, the lattice Boltzmann (LB) method has attracted broad interest in the computational fluid dynamics and the numerical heat transfer communities, primarily due to its kinetic nature making it appropriate for modeling complex multiphase transport phenomena. More importantly, the LB method fits well with parallel computing due to its locality feature, which is required for large-scale engineering applications. In this article, we review the LB method for gas–liquid two-phase flows, coupled fluid flow and mass transport in porous media, and particulate flows. Examples of applications are provided in fuel cells and flow batteries. Further developments of the LB method are also outlined.

Keywords Lattice Boltzmann method · Transport phenomena · Multiphase flow · Fuel cells · Flow batteries

1 Introduction

Electrochemical systems such as fuel cells and flow batteries typically involve fluid flows, heat/mass transport and electrochemical reactions that occur at macro-scale, meso-scale, and nano-scale. The performance and reliability of these technologies depend heavily on our understanding of these complex multiscale transport phenomena, which highlight the demand for accurate predictive approaches. With the emergence of supercomputers in the 1960s, various numerical methods, such as the finite volume (FV) method, finite element (FE) method, lattice Boltzmann (LB) method, dissipative particle dynamic (DPD) method, molecular dynamics (MD) method, and density functional theory (DFT) method, have aided both fundamental research and applied research in mechanical engineering, aerospace engineering, chemical engineering, biological engineering, and energy engineering. Among these numerical methods, the LB method stands out as a powerful tool for simulating fluid flows and associated transport phenomena. The LB method is based on a description of particle density distribution that originated from Boltzmann kinetic theory, and practically predicts hydrodynamic behavior on a continuum scale, which allows for incorporating the mesoscopic physical pictures whilst the physical laws at macroscale can be recovered with low computational cost.

Since the emergence of the LB method, its ability to simulate complex flows has attracted broad interest in the computational fluid dynamics and numerical heat transfer communities [1–10]. In this review, we present the advances of the LB model for gas–liquid two-phase flows, coupled fluid flow and mass transport in porous media, and particulate flows with a focus on fuel cells and flow batteries. The remainder of this paper is organized as follows: Sect. 2

✉ Tianshou Zhao
metzhao@ust.hk

Ao Xu
axu@connect.ust.hk

Wei Shyy
weishyy@ust.hk

¹ HKUST Energy Institute, Department of Mechanical and Aerospace Engineering, The Hong Kong University of Science and Technology, Hong Kong, China

describes the transport phenomena in fuel cells and flow batteries; Sect. 3 introduces the basic LB formulation; Sects. 4–6 review the LB model for gas–liquid two-phase flows, for coupled fluid flow and mass transport in porous media, and for particulate flows, respectively; Sect. 7 reviews the applications of the LB model in simulating transport phenomena in fuel cells and flow batteries. Finally, the summary and outlook are given in Sect. 8.

2 General description of transport phenomena in fuel cells and flow batteries

2.1 Gas–liquid two-phase flows in fuel cells

Proton exchange membrane fuel cells (PEMFCs) are energy conversion devices that convert chemical energy to electrical energy. Figure 1 illustrates a typical PEMFC system, which consists of a proton exchange membrane sandwiched by anode and cathode compartments [11, 12]. Both the anode and the cathode include a flow channel, a gas diffusion layer, and a catalyst layer. The membrane conducts protons and insulates electrons between the anode and the cathode; the flow channels supply uniformly feeds of gas fuels; the diffusion layers provide support to the corresponding catalyst layer and conduct electrons to the current collector; the catalyst layers provide triple-phase boundaries for the electrochemical reactions and facilitate the simultaneous transport of protons, electrons, reactants, and products. The electrochemical reaction on the anode is

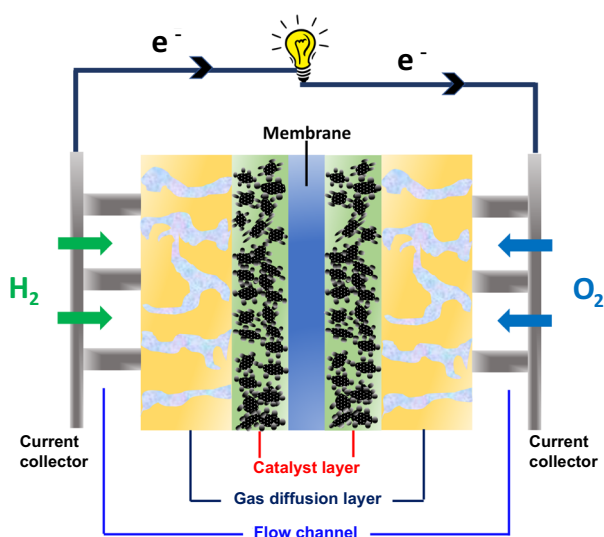
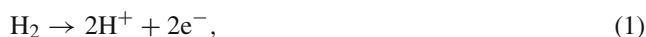
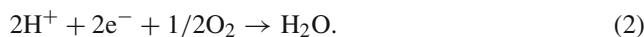


Fig. 1 Schematic illustration of a proton exchange membrane fuel cell system

and the electrochemical reaction on the cathode is



Thus, the overall reaction in the PEMFC is



On the anode, humidified hydrogen is supplied to the catalyst layer where it can be further oxidized to generate electrons and protons, while on the cathode, humidified air is supplied to the catalyst layer, where oxygen reacts with the protons and electrons to form water. At high current density operation, the excessive liquid water produced on the cathode may block the porous pathway in the catalyst layer and the gas diffusion layer, thus hindering the transport of oxygen to the reaction sites. Even worse, the unavoidable liquid water may cover the electrochemically active site in the catalyst layer, thus further decreasing the fuel cell's performance. These phenomena are known as "water flooding". Water flooding also causes transport issues in the flow channel such as channel blockage, which increases the pressure drop. Similar water flooding issues exist in direct methanol fuel cells (DMFCs) as well [13]. In short, on both the anode and the cathode, the transport phenomena involve gas–liquid two-phase flows in the porous media and in the flow channels.

2.2 Coupled fluid flow and mass transport in aqueous redox flow batteries

Flow batteries are energy storage devices that store the intermittent power generated from solar and wind. Figure 2 illustrates a typical aqueous redox flow battery system, which is a sandwiched structure consisting of positive and negative porous carbon electrodes separated by an ion-exchange membrane [14]. The electrolytes containing the dissolved active species are stored in external tanks and circulated through the porous electrodes, where electrochemical reactions occur to store or release electricity. As the energy-storage tanks are separated from the power pack, the stored energy can be scaled independently of power to meet the capacity requirements. The electrochemical reaction at the positive electrode can be expressed as



while the electrochemical reaction at the negative electrode can be expressed as



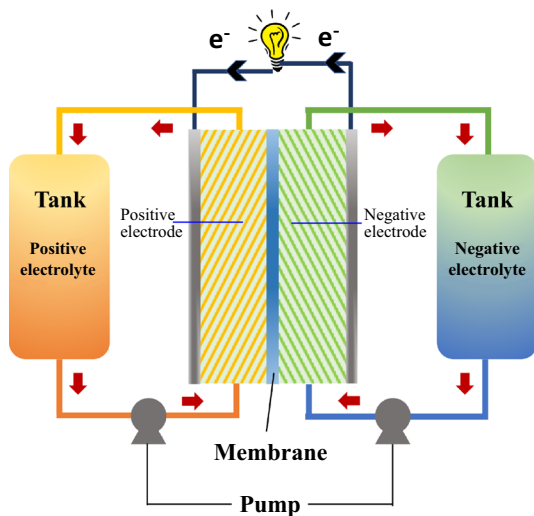


Fig. 2 Schematic illustration of an aqueous redox flow battery system

Depending on the selection of active species for electrochemical reactions at the positive and negative electrodes, various types of aqueous redox flow batteries are available, such as all-vanadium redox flow batteries (VRFBs), iron-chromium redox flow batteries (ICRFBs), polysulphide/bromine flow batteries and so on [15]. In these flow batteries, the electrolyte is pumped from the external tank to the porous electrode. Then, reactants in the electrolyte are dispersed from the electrode inlet and adsorbed onto the surface of electrode pores to participate in electrochemical reactions. Afterwards, the products are desorbed from the reactive surfaces and dispersed in the electrolyte further cycling back to the tank. Meanwhile, the ionic current density resulting from the transport of ions in the liquid electrolyte is in balance with the electronic current density resulting from the transport of electrons through the solid matrix of the porous electrodes. In short, the transport processes in both the positive and negative porous electrodes involve coupled liquid electrolyte flow, mass transport, ion transport, electron transport, and electrochemical reactions.

2.3 Particulate flows in suspension redox flow batteries

The suspension redox flow battery is another type of flow battery, which differs from aqueous redox flow batteries in that in suspension flow batteries the active material is suspended, rather than dissolved in a solution [16]. Figure 3 illustrates a typical suspension redox flow battery system, which shows a similar architecture to aqueous redox flow batteries introduced in Sect. 2.2. In suspension electrodes, there are insoluble charge storing active materials and conductive additives, together with solution electrolytes containing liq-

uid ions. The electrons transport through the formation of percolation networks of agglomerated particles. Because the concentration of active species is much increased in suspension redox flow batteries compared with that in aqueous redox flow batteries, the energy density limitation of aqueous redox flow batteries can be overcome.

The size, shape, and composition of both active material particles and conductive material particles are intrinsically coupled, and affect the rheology and the transport properties of the suspension fluid. Typically, the active material content is between 5–25 wt%. Although further increasing the loading of active material particles will gain higher energy density, the increase in the viscosity of the suspension results in a substantial penalty. Meanwhile, the conductive additives also increase the overall suspension viscosity, even though it is needed to facilitate efficient electron and charge percolation. Thus, there are inherent trade-offs to creating highly conductive percolation pathways and rheological properties. In short, the transport processes in the suspension electrodes involve the particulate flows of active material particles and conductive material particles, and both are inherently coupled with electrochemical reactions.

Based on the above review, first-principle-based modeling techniques capable of handling multiphase and coupled momentum, heat and mass transport are highly desirable to help address the challenges at hand.

3 Basic LB formulations

3.1 The collision operator and the forcing scheme

The LB method traces its root to cellular automata (CA) which were conceived by John von Neumann in the 1940s. In CA, individual cells exist in a state 0 or 1 on a discretized space. At each time step, these cells update their states following a rule that is affected by their neighbors' states. A systematical study on cellular automata was conducted by Wolfram [17] in 1983. In 1986, Frisch et al. [18] took a major step forward by applying CA to fluid systems, and proposed lattice gas cellular automata (LGCA) for the Navier–Stokes equations. The use of a triangular grid restored some of the symmetry required to properly simulate the fluids. However, the LGCA suffers from high statistical noise and lacks Galilean invariance. The next major step was taken by McNamara and Zanetti [19] in 1988. To eliminate the statistical noise of the LGCA, they replaced the Boolean variable in LGCA with a real-valued distribution function. Then a major simplification was introduced by Qian et al. [20] in 1992, who adopted a single-relaxation-time collision model, leading to the lattice Bhatnagar–Gross–Krook model, which is one of the most popular LB models used today. As mentioned above, the LB method originated from CA. On the

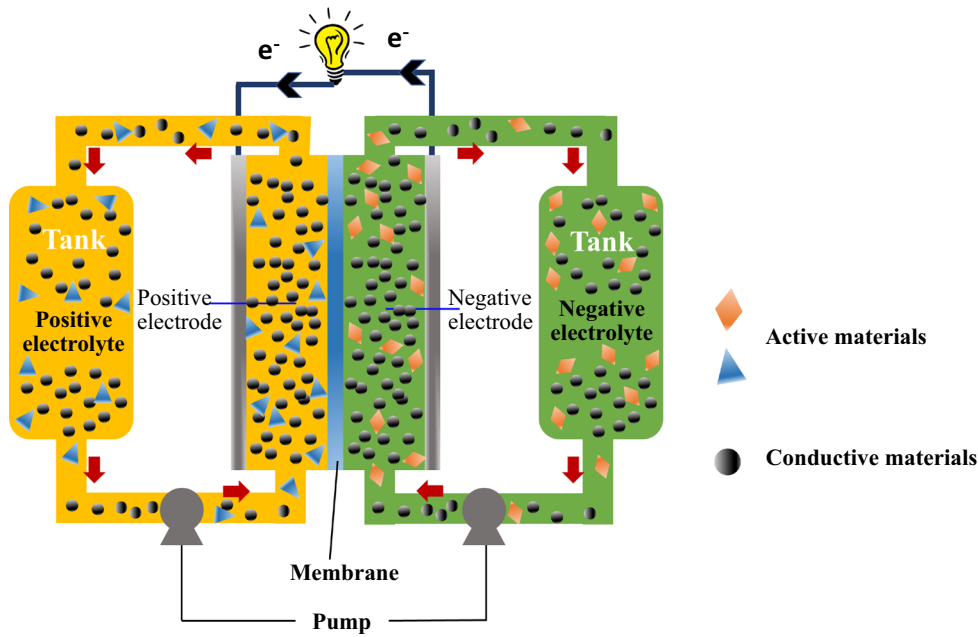


Fig. 3 Schematic illustration of a suspension redox flow battery system

other hand, in 1997, He and Luo [21] proved that the lattice Boltzmann equation can be derived from the continuous Boltzmann equation. The starting point is the Boltzmann equation with the Bhatnagar–Gross–Krook (BGK) approximation [22–24],

$$\frac{\partial f(\mathbf{x}, \boldsymbol{\xi}, t)}{\partial t} + \boldsymbol{\xi} \cdot \nabla f(\mathbf{x}, \boldsymbol{\xi}, t) = -\frac{1}{\tau} \left[f(\mathbf{x}, \boldsymbol{\xi}, t) - f^{(\text{eq})}(\mathbf{x}, \boldsymbol{\xi}, t) \right], \quad (6)$$

where $f^{(\text{eq})}(\mathbf{x}, \boldsymbol{\xi}, t)$ is the Maxwellian distribution function. Expanding $f^{(\text{eq})}(\mathbf{x}, \boldsymbol{\xi}, t)$ into a Taylor series in terms of the fluid velocity for low Mach number flows (i.e., $|\mathbf{u}|/\sqrt{RT} \ll 1$), then

$$f^{(\text{eq})}(\mathbf{x}, \boldsymbol{\xi}, t) = \frac{\rho}{(2\pi RT)^{D/2}} \exp\left(-\frac{\boldsymbol{\xi}^2}{2RT}\right) \times \left[1 + \frac{\boldsymbol{\xi} \cdot \mathbf{u}}{RT} + \frac{(\boldsymbol{\xi} \cdot \mathbf{u})^2}{2RT} - \frac{|\mathbf{u}|^2}{2RT} \right]. \quad (7)$$

Discretizing the velocity space $\boldsymbol{\xi}$ into a discrete velocity set $\{\mathbf{e}_i\}$ under the constraint

$$\int \boldsymbol{\xi}^k f^{(\text{eq})}(\mathbf{x}, \boldsymbol{\xi}, t) d\boldsymbol{\xi} = \sum_i \omega_i \mathbf{e}_i^k f^{(\text{eq})}(\mathbf{x}, \mathbf{e}_i, t), \quad 0 \leq k \leq 3, \quad (8)$$

allows the Navier–Stokes equations to be obtained in the low Mach number limit. Here ω_i and \mathbf{e}_i are the weights and points

of the numerical quadrature. Define a discrete distribution function $f_i(\mathbf{x}, t)$, which satisfies

$$\frac{\partial f_i(\mathbf{x}, t)}{\partial t} + \mathbf{e}_i \cdot \nabla f_i(\mathbf{x}, t) = -\frac{1}{\tau} \left[f_i(\mathbf{x}, t) - f_i^{(\text{eq})}(\mathbf{x}, t) \right], \quad (9)$$

where $f_i^{(\text{eq})}(\mathbf{x}, t) = \omega_i f^{(\text{eq})}(\mathbf{x}, \mathbf{e}_i, t)$. Integrating the above equation from t to $t + \delta_t$ along the characteristic line and assuming the collision term is constant during this interval, the evolution equation of the LB model can be obtained as

$$f_i(\mathbf{x} + \mathbf{e}_i \delta_t, t + \delta_t) - f_i(\mathbf{x}, t) = \Omega_i^{\text{LBGK}}, \quad (10)$$

where $\Omega_i^{\text{LBGK}} = -\frac{1}{\tau} [f_i(\mathbf{x}, t) - f_i^{(\text{eq})}(\mathbf{x}, t)]$. Here, the Ω_i^{LBGK} is known as the lattice Bhatnagar–Gross–Krook (LBGK) collision operator [20]. Meanwhile, since this collision operator relies on only a single relaxation parameter, it is also known as the single-relaxation-time (SRT) collision operator. The fluid density and velocity can then be obtained from the moments of discrete distribution function as

$$\rho(\mathbf{x}, t) = \sum_i f_i(\mathbf{x}, t), \quad \rho(\mathbf{x}, t) \mathbf{u}(\mathbf{x}, t) = \sum_i \mathbf{e}_i f_i(\mathbf{x}, t). \quad (11)$$

One drawback of the LBGK collision operator is that it suffers from server numerical instability at high Reynolds numbers. An alternative collision operator is the multiple-relaxation-time (MRT) collision operator [25, 26]. The MRT collision operator is defined as

$$\Omega_i^{\text{MRT}} = -(\mathbf{M}^{-1}\mathbf{SM})_{ij}[f_j(\mathbf{x}, t) - f_j^{(\text{eq})}(\mathbf{x}, t)]. \tag{12}$$

In the MRT model, the density distribution function f_i and its equilibrium $f_i^{(\text{eq})}$ can be projected onto the moment space with the aid of a transformation matrix \mathbf{M} . Then, the evolution equation of the LB model is rewritten as

$$\mathbf{m}^* = \mathbf{m} - \mathbf{S}(\mathbf{m} - \mathbf{m}^{(\text{eq})}). \tag{13}$$

Here, \mathbf{S} is a relaxation matrix. The macroscopic density ρ and velocity \mathbf{u} in the MRT model can be obtained similarly to their counterparts in the LBGK model. Simulation results of both single and multiphase flows have demonstrated the superior numerical stability of the MRT collision operator over the LBGK collision operator.

In practice, fluid flows are usually exposed to external or internal forces, such as gravity or intermolecular interactions, thus it is essential to include the body force in the LB equation to describe such flows. In the continuous Boltzmann equation, it is quite straightforward to add the body force \mathbf{F} , as

$$\frac{\partial f(\mathbf{x}, \boldsymbol{\xi}, t)}{\partial t} + \boldsymbol{\xi} \cdot \nabla f(\mathbf{x}, \boldsymbol{\xi}, t) + \mathbf{F}(\mathbf{x}, t) \cdot \nabla_{\boldsymbol{\xi}} f(\mathbf{x}, \boldsymbol{\xi}, t) = \Omega_i. \tag{14}$$

In the lattice Boltzmann equation, however, the forcing term cannot be employed straightforwardly because particle velocity is discretized. To account for the forcing term in the LB equation, a forcing term F'_i in velocity space is usually added into the time evolution of the density distribution function

$$f_i(\mathbf{x} + \mathbf{e}_i \delta_t, t + \delta_t) - f_i(\mathbf{x}, t) = \Omega_i + \delta_t F'_i. \tag{15}$$

Obviously, F'_i should depend on the body force \mathbf{F} .

A variety of discrete forcing schemes have been developed; one may refer to Guo and Shu [3], and Huang et al. [27] for a comprehensive comparison. Here, only Guo’s forcing scheme [28,29] is reviewed because it has shown superior numerical stability and accuracy in simulating incompressible single-phase flows [27]. Guo et al. [28] proposed a moment expansion scheme, which is written as

$$F'_i = \omega_i \left(1 - \frac{1}{2\tau} \right) \left[\frac{\mathbf{e}_i \cdot \mathbf{F}}{c_s^2} + \frac{(\mathbf{u}\mathbf{F} + \mathbf{F}\mathbf{u}) : (\mathbf{e}_i \mathbf{e}_i - c_s^2 \mathbf{I})}{2c_s^4} \right]. \tag{16}$$

Extending the above scheme to the MRT LB equation [29], the evolution equation with a forcing term is written as

$$f_i(\mathbf{x} + \mathbf{e}_i \delta_t, t + \delta_t) - f_i(\mathbf{x}, t) = -(\mathbf{M}^{-1}\mathbf{SM})_{ij}[f_j(\mathbf{x}, t) - f_j^{(\text{eq})}(\mathbf{x}, t)] + \delta_t \mathbf{M}^{-1} \hat{\mathbf{F}}, \tag{17}$$

where $\hat{\mathbf{F}}$ represents the moments of the forcing term in the moment space, which can be expressed as

$$\hat{\mathbf{F}} = \left(\mathbf{I} - \frac{1}{2}\mathbf{S} \right) \mathbf{M} \bar{\mathbf{F}}. \tag{18}$$

Here, $\bar{\mathbf{F}}$ is related to the body forces \mathbf{F} as

$$\bar{F}_i = \omega_i \left[\frac{\mathbf{e}_i \cdot \mathbf{F}}{c_s^2} + \frac{(\mathbf{u}\mathbf{F} + \mathbf{F}\mathbf{u}) : (\mathbf{e}_i \mathbf{e}_i - c_s^2 \mathbf{I})}{2c_s^4} \right]. \tag{19}$$

Then, the macroscopic fluid density and velocity are calculated as

$$\begin{aligned} \rho(\mathbf{x}, t) &= \sum_i f_i(\mathbf{x}, t), \\ \rho(\mathbf{x}, t) \mathbf{u}(\mathbf{x}, t) &= \sum_i \mathbf{e}_i f_i(\mathbf{x}, t) + \frac{\delta_t}{2} \mathbf{F}(\mathbf{x}, t). \end{aligned} \tag{20}$$

3.2 Parallel implementation of the LB method

To pursue simulations with faster speeds so that larger physical domains or higher computational resolutions can be achieved, parallel computing techniques are essential in the application of numerical methods for practical engineering problems. Thanks to the localized nature of the LB method, it shows superior capability to fit parallel computing frameworks, including Open Multi-Processing (OpenMP), Message Passing Interface (MPI), Open Accelerator (OpenACC), and Compute Unified Device Architecture (CUDA). When choosing one of the programming standards mentioned above, there is trade-off among the computing facility, the programming effort, and computational efficiency. With regard to the computing facility, OpenMP supports shared memory systems consisting of a single large memory, while MPI supports distributed memory systems consisting of multiple computers with independent memory; OpenACC and CUDA harnesses the power of graphics processing unit (GPU) accelerators, while CUDA works only with NVIDIA’s graphics card. As for the programming effort, both OpenMP and OpenACC are directive programming standards which are easily implemented; MPI and CUDA require substantial changes in the serial code, thus threatening the code correctness, portability, and maintainability. In terms of computational efficiency, usually MPI shows better scalability

than OpenMP, while the sophisticated management of memory in CUDA brings benefits compared with OpenACC. Simulations using the LB method, as with other numerical methods, have been utilizing OpenMP and MPI acceleration since the 1990s. Nowadays, GPU attracts a lot of attention as an emerging computational accelerator due to its combined tremendous computing power and superior memory bandwidth. Many previous efforts have been devoted to CUDA accelerated LB simulation [30–35], and they show good parallel efficiency. Motivated by the requirement that the hardware should have less restriction on practical engineering applications, recently Xu et al. [36] assessed the performance of OpenACC accelerated LB simulations, and the results demonstrate that OpenACC allows a speed-up of around 50–60 times for multiphysics LB simulation with double-precision floating point arithmetic.

4 LB model for gas–liquid two-phase flows

Existing LB models for gas–liquid two-phase flows can be classified into four categories: the color-gradient model proposed by Gunstensen et al. [37] and Grunau et al. [38], the pseudo-potential model proposed by Shan and Chen [39,40], the free-energy model proposed by Swift et al. [41,42], and the phase-field model proposed by He et al. [43].

The color-gradient LB model was proposed by Gunstensen et al. [37] in 1991 and Grunau et al. [38] in 1993, which is based on the work of immiscible two-phase flows for lattice gas cellular automata (LGCA) by Rothman and Keller [44] in 1988. In this model, phase separation is achieved via a re-coloring step. Two distribution functions for red-colored fluid and blue-colored fluid were used to denote the two different fluids. In addition to the standard collision step in LB method, an additional collision operator for generating the surface tension was adopted. The advantage of the color-gradient model is that the viscosity ratio and the surface tension can be varied independently. However, the original color-gradient model is limited to the case of identical densities for immiscible two-phase flows. Huang et al. [45] found that the reason behind this is that unwanted extra terms exist in the recovered Navier–Stokes equations derived from the color-gradient model. To eliminate the unwanted terms, they introduced a source term in the LB equation and a liquid–gas density ratio of order $O(10)$ was achieved. Later, Huang et al. [46] proposed an MRT color-gradient model which can significantly reduce the spurious currents, and their model shows better numerical stability. Recently, Ba et al. [47] also proposed an MRT color-gradient model with an additional source term to recover the Navier–Stokes equations, and two-phase flows with density ratios of order $O(100)$ and Reynolds numbers of order $O(100)$ were simulated.

The pseudo-potential LB model was proposed by Shan and Chen [39,40] in 1993 and 1994. In this model, the fluid interactions among different phases are described by an artificial inter-particle potential. The inter-particle potential is incorporated into the LB equation via a forcing scheme so that phase separation can be achieved. The advantage of the pseudo-potential model is that interfaces can arise, deform, and migrate naturally, thus improving the computational efficiency. However, one should be cautious when applying the original pseudo-potential model due to the following two issues: first, the model is applicable only to low liquid–gas density ratio problems; secondly, the surface tension cannot be varied independently of the density ratio in this model. The efforts to address these issues include incorporating realistic EOS into the model [48], increasing the isotropy order of the interaction force [49,50], modifying the interaction force [51,52], and improving the forcing scheme to incorporate the interaction force into the model [27,53–57]. Recently, Reijers et al. [58] also extended the pseudo-potential model to simulate axisymmetric multiphase flows, which offers significantly lower computational costs than its full counterpart.

The free-energy LB model was proposed by Swift et al. [41,42] in 1995 and 1996. In this model, phase separation is achieved by incorporating a non-ideal equation of state into the pressure tensor. Specifically, the thermodynamics is considered via modifying the second-order moment of the equilibrium density distribution function. The advantage of the free-energy model is that the surface tension can be varied easily. However, the original free-energy model is not Galilean invariant. Inamuro et al. [59] proposed a Galilean-invariant free-energy LB model, but a Poisson equation must be solved, which spoils the locality of the LB method.

The phase-field LB model was proposed by He et al. [43] in 1999. In this model, phase separation is achieved by tracking an order parameter, which has constant value in the bulk phase and varies smoothly across the diffuse-interface region. Two distribution functions and two corresponding LB equations are used to recover the Navier–Stokes equations and the interface tracking equation, respectively. Usually, the Cahn–Hilliard equation [60,61] based on phase-field theory is adopted to capture the phase interface dynamics, while recent advances using the Allen–Cahn equation [62] also show promising applications [63]. It should be noted that in the literature, the free-energy LB model and phase-field LB model are not strictly distinguished. This is because the thermodynamic behavior of a fluid can be expressed by the free energy, which is functional of the order parameter. Here, we classify those models that describing the interface dynamics by an order parameter as phase-field LB models; examples include Inamuro et al. [64], Lee et al. [65], Huang et al. [66], and Shao et al. [67]. The advantage of the phase-field model is that it has solid physical foundations due to its link with

phase-field theory to capture the interface dynamics. Furthermore, it is convenient in simulating axisymmetric multiphase flows [68, 69]. However, to correctly recover the macroscopic equations is a nontrivial thing: Li et al. [70] found that the recovered momentum equation includes an additional force term; Liang et al. [71] found that the Cahn–Hilliard equation cannot be completely recovered. In addition, the implementation of wetting boundary conditions in phase-field method is tricky, since for both the order parameter and the chemical potential, suitable boundary conditions are required [72–74]. In addition, it is worth mentioning that recently Liang et al. [75] made attempts to simulate three-phase incompressible flows based on multicomponent phase-field theory.

As shown above, much progress has been made on these gas–liquid two-phase LB models. Still, the strengths of different models vary for simulating multiphase flows at large density ratios and the capability of maintaining non-diffuse interface thickness for long-time evolution [76]. The Rayleigh–Taylor instability (RTI) problem is a classical benchmark to demonstrate the density ratio effect on multiphase flows. In the RTI problem, a heavier fluid is accelerated against a lighter one with slight perturbation at the interface. The Atwood number (At), which is defined as $At = (\rho_{\text{heavier}} - \rho_{\text{lighter}})/(\rho_{\text{heavier}} + \rho_{\text{lighter}})$, is a main dimensionless parameter to characterize the flow behavior. In addition, the ability of the LB model to simulate multicomponent flows and thermal flows, and the flexibility for implementing wetting boundary conditions in complex geometries, also varies [8, 9, 77]. In the following, we will discuss in detail the formulation and development of only the pseudo-potential LB model, because in terms of personal perspective, we think the practical engineering application of the pseudo-potential LB model in simulating thermal multiphase flows [78–80], multicomponent multiphase flows [81], and multiphase flows in porous media [82–84] is more promising. It is also worth mentioning that there have been some comprehensive reviews of gas–liquid two-phase LB models, such as by Huang et al. [8], Li et al. [9], and Chen et al. [85].

To simulate single-component multiphase flows, the interaction force derived from inter-particle potential to mimic the molecular interactions is adopted as [49, 86]

$$\mathbf{F}_{\text{int}}(\mathbf{x}) = -G\psi(\mathbf{x}) \sum_{i=1}^N w(|\mathbf{e}_i|^2)\psi(\mathbf{x} + \mathbf{e}_i)\mathbf{e}_i, \tag{21}$$

where $\psi(\mathbf{x})$ represents the interaction potential, G represents the interaction strength, and $w(|\mathbf{e}_i|^2)$ are the weights. Yuan and Schaefer [48] suggested incorporating an equation of state (EOS) for non-ideal gases, such as the Carnahan–Starling EOS and the Peng–Robinson EOS, in the interaction potential $\psi(\mathbf{x})$; similarly, Li and Luo [87] reported the use of an artificial piecewise linear EOS. In the pseudo-potential

model, the forcing scheme to incorporate the interaction force will markedly affect the numerical accuracy and stability of the model. In Sect. 3.2, we have introduced Guo’s forcing scheme to incorporate the body force in simulating incompressible single-phase flows, which shows superior numerical accuracy and stability. However, incorporating the force term in the pseudo-potential LB model is much more complex [27, 53, 57, 88]. Here, we review the forcing scheme proposed by Li et al. [54, 55] based on the D2Q9 lattice model, which is capable of achieving large density ratios as well as variable surface tension. The evolution equation of the LB model is

$$\mathbf{m}^* = \mathbf{m} - \mathbf{S}(\mathbf{m} - \mathbf{m}^{(\text{eq})}) + \delta_t \left(\mathbf{I} - \frac{\mathbf{S}}{2} \right) \mathbf{M}\tilde{\mathbf{F}} + \mathbf{C}. \tag{22}$$

For the D2Q9 lattice model, the terms $\mathbf{M}\tilde{\mathbf{F}}$ and \mathbf{C} are given by,

$$\mathbf{M}\tilde{\mathbf{F}} = \begin{bmatrix} 0 \\ 6\mathbf{u} \cdot \mathbf{F} + \frac{12\sigma|\mathbf{F}|^2}{\psi^2\delta_t(s_e^{-1}-0.5)} \\ -6\mathbf{u} \cdot \mathbf{F} - \frac{12\sigma|\mathbf{F}|^2}{\psi^2\delta_t(s_\zeta^{-1}-0.5)} \\ F_x \\ -F_x \\ F_y \\ -F_y \\ 2u_x F_x - 2u_y F_y \\ u_x F_y + 2u_y F_x \end{bmatrix},$$

$$\mathbf{C} = \begin{bmatrix} 0 \\ \frac{3}{2}s_e(Q_{xx} + Q_{yy}) \\ -\frac{3}{2}s_\zeta(Q_{xx} + Q_{yy}) \\ 0 \\ 0 \\ 0 \\ 0 \\ -s_\nu(Q_{xx} - Q_{yy}) \\ -s_\nu Q_{xy} \end{bmatrix}, \tag{23}$$

respectively. Here, σ is introduced to tune the mechanical stability condition; the variables Q_{xx} , Q_{yy} , and Q_{xy} are obtained from

$$\mathbf{Q} = \kappa \frac{G}{2} \psi(\mathbf{x}) \sum_{i=1}^N w(|\mathbf{e}_i|^2)[\psi(\mathbf{x} + \mathbf{e}_i) - \psi(\mathbf{x})]\mathbf{e}_i\mathbf{e}_i, \tag{24}$$

where the parameter κ is introduced to vary the surface tension. The adhesive force between fluid and solid must be considered when the fluids interact with a solid wall. Two types of fluid-solid interaction force have been widely adopted: the density-based interaction force [89, 90] and the pseudo-potential-based interaction force [91]. Li et al. [92]

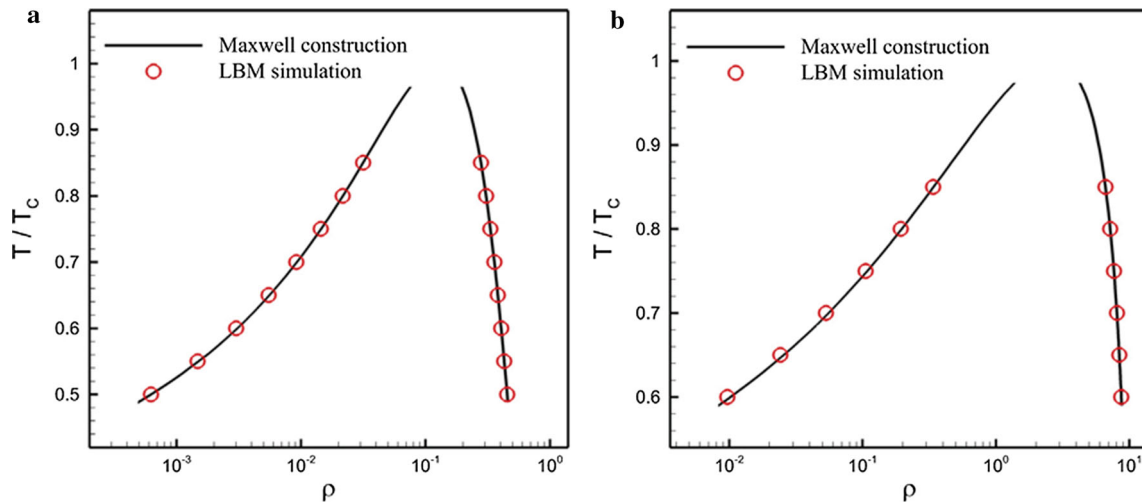


Fig. 4 Coexistence curves obtained from Maxwell construction and LB simulation [56]. Reproduced from Ref. [56] (Copyright 2015, Elsevier). **a** Coexistence curve of the C–S EOS and **b** coexistence curve of the P–R EOS

proposed a pseudo-potential-based fluid-solid interaction force that can vary contact angle, even when the liquid-gas density ratio is large. The adhesive force is written as

$$\mathbf{F}_{\text{ads}}(\mathbf{x}) = -G_{\text{ads}}\psi(\mathbf{x}) \sum_{i=1}^N w(|\mathbf{e}_i|^2)\psi(\mathbf{x})s(\mathbf{x} + \mathbf{e}_i)\mathbf{e}_i, \quad (25)$$

where G_{ads} represents the fluid-solid interaction strength to adjust the contact angle. $s(\mathbf{x})$ is the indicator function, i.e., $s(\mathbf{x}) = 1$ when \mathbf{x} is in solid, and $s(\mathbf{x}) = 0$ when \mathbf{x} is in fluid. With the addition of body force \mathbf{F}_{body} , then the total force \mathbf{F} in Eq. (23) is

$$\mathbf{F} = \mathbf{F}_{\text{int}} + \mathbf{F}_{\text{ads}} + \mathbf{F}_{\text{body}}. \quad (26)$$

Through Chapman–Enskog analysis [56,93], the macroscopic equations obtained from LB equation with the above forcing scheme is

$$\frac{\partial \rho}{\partial t} + \nabla \cdot (\rho \mathbf{u}) = 0, \quad (27a)$$

$$\begin{aligned} \frac{\partial (\rho \mathbf{u})}{\partial t} + \nabla \cdot (\rho \mathbf{u} \mathbf{u}) \\ = -\nabla \cdot (\rho c_s^2 \mathbf{I}) + \nabla \cdot \mathbf{\Pi} + \mathbf{F} - 2G^2 c^4 \sigma \nabla \cdot (|\nabla \psi|^2 \mathbf{I}) \\ - \nabla \cdot \left[\kappa \frac{Gc^4}{6} (\psi \nabla^2 \psi \mathbf{I} - \psi \nabla \nabla \psi) \right], \end{aligned} \quad (27b)$$

where $\mathbf{\Pi}$ is shear stress and is defined as

$$\mathbf{\Pi} = \rho \nu \left[\nabla \mathbf{u} + (\nabla \mathbf{u})^T \right] + \rho \left(\xi - \frac{2}{3} \nu \right) (\nabla \cdot \mathbf{u}) \mathbf{I}. \quad (28)$$

When $\sigma = 0$ and $\kappa = 0$, the standard pressure tensor can be recovered from Eq. (27). The mechanical stability con-

dition is given as $\varepsilon = -2(\alpha + 24G\sigma)/\beta$, where α and β are given by $\alpha = 0$ and $\beta = 3$, respectively [86]. To make the mechanical stability condition approximate the thermodynamic consistency requirement, the parameter ε is suggested to be chosen as $1 < \varepsilon < 2$ [53], while its exact value can be further determined through fitting the Maxwell construction solution [54,56]. Following the above approach to devise two-dimensional models, Xu et al. [56] have devised a three-dimensional pseudo-potential-based LB model with large density ratios as well as variable surface tension. Figure 4 shows the coexistence curves demonstrating that the proposed forcing scheme is capable of achieving thermodynamic consistency and large density ratios; Fig. 5 shows the pressure differences between the inside and outside of a droplet versus the reciprocal of the droplet radius at different values of κ , demonstrating that the proposed forcing scheme is capable of adjusting the surface tension.

To simulate multi-component multiphase flows, the cohesive force acting on the σ th component is [89]

$$\mathbf{F}_{c,\sigma}(\mathbf{x}) = -G_c \rho_\sigma(\mathbf{x}) \sum_{i=1}^N w(|\mathbf{e}_i|^2) \rho_{\bar{\sigma}}(\mathbf{x} + \mathbf{e}_i) \mathbf{e}_i, \quad (29)$$

where σ and $\bar{\sigma}$ represent two different fluid components, and G_c is the cohesion strength. The fluid-solid force acting on the σ th component is

$$\mathbf{F}_{\text{ads},\sigma}(\mathbf{x}) = -G_{\text{ads},\sigma} \rho_\sigma(\mathbf{x}) \sum_{i=1}^N w(|\mathbf{e}_i|^2) s(\mathbf{x} + \mathbf{e}_i) \mathbf{e}_i, \quad (30)$$

where $G_{\text{ads},\sigma}$ can be used to adjust the interaction strength between each fluid and a wall. Huang et al. [94] proposed an elegant formula to determine the contact angle using

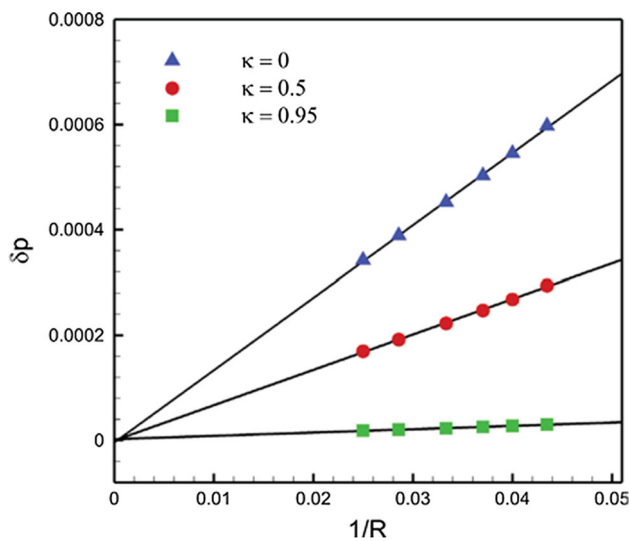


Fig. 5 Validation of the Laplace’s law [56]. Reproduced from Ref. [56] (Copyright 2015, Elsevier)

the adhesion parameters so that a desired fluid-solid contact angle can be achieved, which is written as

$$\cos \theta = \frac{G_{\text{ads},2} - G_{\text{ads},1}}{G_c \frac{\rho_1 - \rho_2}{2}} \tag{31}$$

One issue of the original multicomponent multiphase pseudopotential LB model is that model is limited to a fixed Schmidt number. To address this issue, Chai and Zhao [81] devised a potential-based MRT LB model such that multicomponent flows with different molecular weights can be simulated.

To simulate thermal multiphase flows, either the double distribution function (DDF) approach [79,95–97] or the lattice Boltzmann–finite difference (LB-FD) hybrid approach [80,98,99] can be adopted. In the DDF approach, another distribution function is utilized to solve the energy equation in addition to the distribution function used to solve the flow equation. In the hybrid approach, the LB method is adopted to solve the flow equation together with the finite difference method to solve the energy equation. This hybrid approach was motivated by two reasons. First, the present available LB models cannot solve the target energy equation exactly, particularly when the flow equation includes an additional force term; secondly, the LB method has no obvious advantage over the finite difference method in terms of efficiency when solving the energy equation, because the source term in the energy equation, which is responsible for the phase change, has to be discretized using the finite difference method. Starting from the local balance law for entropy, the temperature equation is given as

$$\rho c_v \frac{DT}{Dt} = \nabla \cdot (\lambda \nabla T) - T \left(\frac{\partial p_{\text{EOS}}}{\partial T} \right)_\rho \nabla \cdot \mathbf{v}, \tag{32}$$

where λ denotes the thermal conductivity and c_v denotes the specific heat at constant volume.

To implement outflow boundary conditions for multiphase flow LB simulations, Lou et al. [100] evaluated the Neumann boundary condition, the extrapolation boundary condition, and the convective boundary condition. They concluded that the convection boundary condition works best among these three types. Similarly, Li et al. [101] investigated the outlet boundary condition for multiphase flows with large liquid-gas density ratios.

5 LB model for coupled fluid flow and mass transport in porous media

Numerical models for fluid flows and associated transport processes in porous media can be classified into two categories according to the physical length scale, namely the representative elementary volume (REV)-scale model and the pore-scale model. The REV-scale model considers the presence of porous media based on empirical relations. For example, the Kozeny–Carman relation is used to estimate permeability, and the Bruggeman relation is used to estimate effective diffusivity. The advantage of the REV-scale model is that it is computationally efficient for modeling physical and chemical processes occurring in porous media. However, the accuracy of REV-scale models rely heavily on the empirical relations. The pore-scale model, on the contrary, allows the consideration of realistic microporous structure, that is, detailed pore geometry is directly resolved. The constitutive closure relations, such as permeability or effective diffusivity as a function of porosity, can be calculated with the aid of pore-scale fluid flow/mass transfer information. The advantage of the pore-scale model is that it can truly reflect the geometrical effect of a porous medium without adopting an empirical relation as that used in REV-scale model. However, the computational cost of pore-scale models is usually very high, which limits their wide application based on today’s lab-scale computational resources.

In REV-scale LB models, the porous medium is treated as a continuous medium. The porosity, the permeability and other statistical properties of the porous medium are essential input values in these models. A number of empirical mathematical models have been proposed to describe the fluid flows in a porous medium, such as Darcy’s model, the Brinkman model, and the generalized model [102]. Darcy’s model is appropriate when the Reynolds number of flow in the porous medium is small, and its mathematical formulation is

$$\nabla p = -\frac{\mu}{K} \mathbf{u}, \tag{33}$$

where K is the permeability of the porous medium. The Brinkman model extends the Darcy model by adding a viscous term, which is written as

$$\nabla p = -\frac{\mu}{K}\mathbf{u} + \mu_e \nabla^2 \mathbf{u}, \tag{34}$$

where μ_e represents an effective viscosity which can be different from the fluid viscosity. The generalized model includes the linear resistance (Darcy) term, the viscous (Brinkman) term, together with the non-linear resistance (Forchheimer) term. The governing equation is written as

$$\nabla \cdot \mathbf{u} = 0, \tag{35a}$$

$$\frac{\partial \mathbf{u}}{\partial t} + (\mathbf{u} \cdot \nabla) \left(\frac{\mathbf{u}}{\varepsilon} \right) = -\frac{1}{\rho} \nabla (\varepsilon p) + \nu_e \nabla^2 \mathbf{u} + \mathbf{F}, \tag{35b}$$

where \mathbf{u} is the apparent velocity, p is the apparent pressure, ν_e is the effective viscosity, \mathbf{F} is the total force given as

$$\mathbf{F} = -\frac{\varepsilon \nu}{K} \mathbf{u} - \frac{\varepsilon F_\varepsilon}{\sqrt{K}} |\mathbf{u}| \mathbf{u} + \varepsilon \mathbf{G}. \tag{36}$$

Here, ν denotes the fluid viscosity, and \mathbf{G} denotes the external body force. The structure function F_ε depends on the permeability K and the porosity ε .

In 2002, Guo and Zhao [103] devised an LB model to solve the above generalized equations. In this model, the evolution equation is written as

$$\begin{aligned} & f_i(\mathbf{x} + \mathbf{e}_i \delta_t, t + \delta_t) - f_i(\mathbf{x}, t) \\ &= -\frac{1}{\tau} \left[f_i(\mathbf{x}, t) - f_i^{(eq)}(\mathbf{x}, t) \right] + \delta_t F'_i, \end{aligned} \tag{37}$$

where the equilibrium distribution includes porosity ε to consider the presence of a solid porous matrix

$$f_i^{(eq)} = \omega_i \rho \left[1 + \frac{\mathbf{e}_i \cdot \mathbf{u}}{c_s^2} + \frac{\mathbf{u}\mathbf{u} : (\mathbf{e}_i \mathbf{e}_i - c_s^2 \mathbf{I})}{2\varepsilon c_s^4} \right] \tag{38}$$

and the force term also includes the effect of a porous structure,

$$F'_i = \omega_i \rho \left(1 - \frac{1}{2\tau} \right) \left[\frac{\mathbf{e}_i \cdot \mathbf{F}}{c_s^2} + \frac{\mathbf{u}\mathbf{F} : (\mathbf{e}_i \mathbf{e}_i - c_s^2 \mathbf{I})}{\varepsilon c_s^4} \right]. \tag{39}$$

The macroscopic velocity \mathbf{u} is calculated as

$$\mathbf{u} = \frac{\mathbf{v}}{c_0 + \sqrt{c_0^2 + c_1 |\mathbf{v}|}}, \tag{40}$$

where \mathbf{v} is a temporary velocity and it is defined as

$$\rho \mathbf{v} = \sum_i \mathbf{e}_i f_i + \frac{\delta_t}{2} \varepsilon \rho \mathbf{G}. \tag{41}$$

Here, \mathbf{G} is the external body force. The parameters c_0 and c_1 are given as

$$c_0 = \frac{1}{2} \left(1 + \varepsilon \frac{\delta_t}{2} \frac{\nu}{K} \right), \quad c_1 = \varepsilon \frac{\delta_t}{2} \frac{F_\varepsilon}{\sqrt{K}}. \tag{42}$$

To solve the coupled fluid flow and heat transfer problem in porous media, an additional energy equation is needed. Assuming a local thermal equilibrium exists between the fluids and the solid matrix, then the energy equation is

$$\sigma \frac{\partial T}{\partial t} + \mathbf{u} \cdot \nabla T = \nabla \cdot (\alpha_m \nabla T), \tag{43}$$

where $\sigma = \varepsilon + (1 - \varepsilon) \rho_s c_{ps} / (\rho_f c_{pf})$ describes the solid-fluid heat capacity ratio, and $\alpha_m = k_m / (\rho_f c_{pf})$ is the effective thermal diffusivity.

In 2005, Guo and Zhao [104] extended their previous LB model [103] to consider the coupled fluid flow and heat transfer problem in porous media. The LB equation for fluid flow is the same as shown in Eq. (37); while another distribution function g_i is adopted to solve the energy equation, which is written as

$$g_i(\mathbf{x} + \mathbf{e}_i \delta_t, t + \delta_t) - g_i(\mathbf{x}, t) = -\frac{1}{\tau_g} \left[g_i(\mathbf{x}, t) - g_i^{(eq)}(\mathbf{x}, t) \right]. \tag{44}$$

The equilibrium distribution function is given by

$$g_i^{(eq)}(\mathbf{x}, t) = \omega_i T \left(1 + \frac{\mathbf{e}_i \cdot \mathbf{u}}{c_s^2} \right). \tag{45}$$

The fluid temperature T is calculated as

$$\sigma T = \sum_i g_i. \tag{46}$$

In the work of Guo and Zhao [103, 104], the collision operator in the LB equation is the LBGK collision operator. Motivated by the fact that the MRT collision operator has shown superior numerical accuracy and stability in a variety of applications, Liu et al. [105] proposed an MRT-LB model for convection heat transfer in porous media following the above approach to devise the REV-scale LB model. To increase the numerical stability, Wang et al. [106] also proposed a local computing scheme to calculate the shear rate and the temperature gradient. In addition, it is worth mentioning that the above REV-scale LB models have also

been extended to study axisymmetric thermal flows [107] and electro-osmotic flows [108] through porous media.

In the pore-scale LB model, the fluid flow is described by the Navier–Stokes equation, the heat/mass transport can be described by a convection–diffusion equation (CDE), the electric potential of ions can be described by the Poisson–Boltzmann equation (PBE), and the presence of porous medium is treated as solid obstacles. Despite the pore geometry being complex and irregular, in the LB method, the solid boundary condition can be achieved easily by following the bounce-back rule, which greatly reduces the programming effort. What is more, recent advancements in parallel programming using both the central processing unit (CPU) and the graphics processing unit (GPU) architectures facilitate large-scale engineering applications [109]. On the other hand, the LB method has been extended as a mathematical tool to solve CDEs [110–119] and PBEs [120–127], indicating it is viable for simulating coupled fluid flow and heat/mass transport processes. For example, in 2013, Chai and Zhao [115] proposed an LB model for CDEs, and through Chapman–Enskog analysis they proved that the CDE can be recovered correctly from their model. Later, Chai and Zhao [116] extended their model to the MRT version, and proposed a nonequilibrium scheme for computing the heat/mass flux. For CDEs with variable coefficients, Li et al. [117] proposed an LBGK model for n -dimensional steady CDE through modifying the equilibrium distribution function; later, Li et al. [118] further proposed to achieve variable coefficients in CDEs through the introduction of an auxiliary distribution function in the LB model. Recently, Chai et al. [128] devised an MRT LB model for general nonlinear anisotropic CDEs based on the work of Shi and Guo [110].

A broad interest in applying pore-scale LB models is to predict the transport properties, including permeability [129–131], effective thermal conductivity [132–135], heat transfer coefficient, effective mass diffusivity [136–138], and mass transfer coefficient. In this aspect, one should be cautious when choosing the LBGK collision operator, as Pan et al. [129] reported that the permeability calculated based on LBGK model depends on the relaxation time. To eliminate this unphysical effect, the MRT model is recommended with specific relaxation time parameters. Recently, Chai et al. [138] obtained a similar conclusion when calculating effective diffusivity in porous media.

6 LB model for particulate flows

Numerical approaches for studying suspensions are generally classified into three categories based on the levels of detail and accuracy required [139, 140]. The first category is the two-fluid approach, i.e., both solid and fluid phases are described as interpenetrating continua. The sec-

ond category is the point-particle approach, in which the solid particle is treated as a discrete mass point and the fluid phase is considered as a continuum. In the point-particle approach, the drag closure is used for fluid–solid coupling. The third category is the particle-resolved approach, where fluid flow is solved through imposing appropriate boundary conditions at the particle surfaces, while the velocities and positions of the particles are determined by explicitly computing the fluid forces acting on the particles. While the particle-resolved simulation is based on first-principles, the computational cost limits the suspension system that can be simulated. Thus, there is a trade-off between computational efforts and resolving down to a fine spatial and time scale.

In the particle-resolved simulations, the motion of particles and fluid must be coupled together. These simulation techniques contains four essential parts: simulating fluid flows governed by the Navier–Stokes equation, simulating particle motions governed by Newton’s second law and Euler’s second law, handling the boundary condition at the moving particle’s surface, and modeling fluid–particle and particle–particle interactions. For simulation of fluid flows governed by the Navier–Stokes equation, we have reviewed the LB formulations in Sect. 3; for simulation of particles motions, at each time step, the Euler method or Runge–Kutta method can be applied for solving the following ordinary differential equations:

$$M_p \frac{d\mathbf{U}(t)}{dt} = \mathbf{F}(t), \quad (47)$$

$$\mathbf{I}_p \cdot \frac{d\boldsymbol{\Omega}(t)}{dt} + \boldsymbol{\Omega}(t) \times [\mathbf{I}_p \cdot \boldsymbol{\Omega}(t)] = \mathbf{T}(t), \quad (48)$$

where M_p is the mass and \mathbf{I}_p is the inertial tensor of the solid particle. \mathbf{U} is the particle center velocity, $\boldsymbol{\Omega}$ is the particle angular velocity. \mathbf{F} is the total force and \mathbf{T} is the total torque exerted on the solid particle. For homogenous spherical particles, the nonlinear term $\boldsymbol{\Omega}(t) \times [\mathbf{I}_p \cdot \boldsymbol{\Omega}(t)]$ vanishes, which greatly simplifies solving Eq. (48). However, for irregularly shaped particles, the solution of Eq. (48) cannot be obtained straightforwardly due to its inherent singularity. For example, in the case of simulating ellipsoid particles, four quaternion parameters should be adopted as generalized coordinates [141–147].

At the particle’s surface, usually the no-slip boundary condition should be guaranteed. In the LB method, the fluid–solid interface can be easily implemented in regular Cartesian grids, thereby improving the computational efficiency for moving particle simulations. Specifically, the no-slip boundary condition can be achieved through modifications to the density distribution function encountering the surface. Although the basic implementation of a no-slip boundary condition is rather simple [148, 149], Lishchuk et al. [150]

found that the simple bounce-back scheme requires an empirical correction for the effective hydrodynamic radius. To obtain more accurate curved wall boundaries, the interpolated bounce-back scheme can be adopted. Recently, Peng et al. [151] compared various interpolated bounce-back schemes, including the scheme proposed by Bouzidi et al. [152] (or the simplified version proposed by Lallemand and Luo [153]), Mei et al. [154,155], Yu et al. [10], and Chun and Ladd [156]. They concluded that the force fluctuation on the particle can be reduced with the aid of quadratic interpolation schemes, and Bouzidi et al.’s scheme appears to perform best [151]. In addition to particulate flow with no-slip boundary conditions at the fluid-solid interface, recently Tao et al. [157] investigated the dynamics of slippery particles suspended in Newtonian fluids.

To calculate the force and torque exerted by the fluid on the solid particle, the momentum-exchange method [158] is suggested to be adopted due to its simplicity and robustness compared with stress integration method [159]. In the momentum-exchange method, the hydrodynamic force acting on the solid surface is calculated by summing up the local momentum exchange of the fluid parcels during the bounce back process at the fluid solid interface over boundary links. Because the original momentum-exchange method proposed by Ladd [148,149] lacks local Galilean invariance [160], several modified momentum-exchange methods were proposed. In 2013, Chen et al. [161] proposed to calculate the total force \mathbf{F} and total torque \mathbf{T} as

$$\mathbf{F} = \sum_{\mathbf{x}_f} \sum_{i_{bl}} \left\{ [f_i^+(\mathbf{x}_f, t) + f_i(\mathbf{x}_f, t + \delta_t)] \mathbf{e}_i - 2\omega_i \rho_0 \frac{\mathbf{e}_i \cdot \mathbf{u}_w}{c_s^2} \mathbf{u}_w \right\}, \tag{49a}$$

$$\mathbf{T} = \sum_{\mathbf{x}_f} \sum_{i_{bl}} (\mathbf{x}_w - \mathbf{x}_c) \times \left\{ [f_i^+(\mathbf{x}_f, t) + f_i(\mathbf{x}_f, t + \delta_t)] \mathbf{e}_i - 2\omega_i \rho_0 \frac{\mathbf{e}_i \cdot \mathbf{u}_w}{c_s^2} \mathbf{u}_w \right\}, \tag{49b}$$

where f_i^+ denotes post-collision distribution function, and f_i denotes the distribution function associated with the velocity $\mathbf{e}_i = -\mathbf{e}_i \cdot \mathbf{x}_c$ denotes the center position of the solid particle. Later, in 2014, Wen et al. [162] proposed to calculate the total force \mathbf{F} and total torque \mathbf{T} as

$$\mathbf{F} = \sum_{\mathbf{x}_f} \sum_{i_{bl}} [f_i^+(\mathbf{x}_f, t) (\mathbf{e}_i - \mathbf{u}_w) - f_i(\mathbf{x}_f, t + \delta_t) (\mathbf{e}_i - \mathbf{u}_w)], \tag{50a}$$

$$\mathbf{T} = \sum_{\mathbf{x}_f} \sum_{i_{bl}} (\mathbf{x}_w - \mathbf{x}_c) \times [f_i^+(\mathbf{x}_f, t) (\mathbf{e}_i - \mathbf{u}_w) - f_i(\mathbf{x}_f, t + \delta_t) (\mathbf{e}_i - \mathbf{u}_w)]. \tag{50b}$$

Peng et al. [151] further demonstrated that using these two methods can correctly simulate the Segré–Silberberg phenomenon (as illustrated in Fig. 6 [163]), whereas the convective momentum-exchange method fails. What is more, the simulation results show that the difference between these two methods is negligible. Recently, Peng et al. [164] argued that the origin of Galilean invariance violation in the presence of a moving solid-fluid interface is due to the bounce-back scheme in addition to the momentum exchange method used, and they demonstrated that their newly proposed bounce-back scheme can significantly improve the accuracy of the simulated flow velocity in turbulent flows.

To prevent overlap between two particles or overlap between a particle and a wall when their distance is small, artificial repulsive force models, such as the spring force

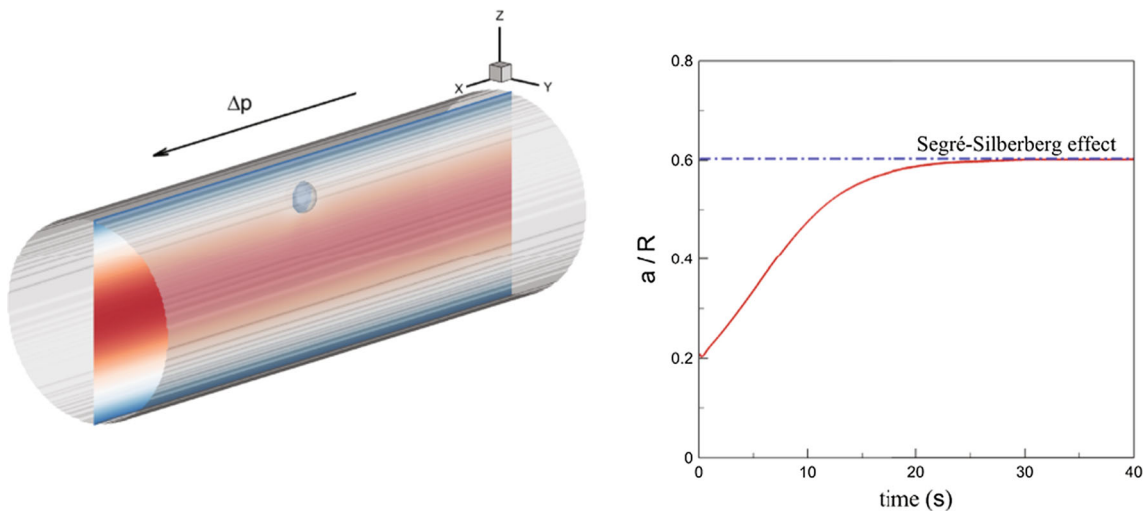


Fig. 6 A neutrally buoyant particle migrates in a pressure driven tube illustrating the Segré–Silberberg phenomenon [163]. Reproduced from Ref. [163] (Copyright 2016, Elsevier)

model [165] and the lubrication force model [166], should be adopted. In the spring force model, the repulsive force is given as

$$\mathbf{F}_R = \begin{cases} \mathbf{0}, & \text{if } |\mathbf{x}_s| > s, \\ \frac{C}{\varepsilon_w} \left(\frac{|\mathbf{x}_s| - s}{s} \right)^2 \frac{\mathbf{x}_s}{|\mathbf{x}_s|}, & \text{if } |\mathbf{x}_s| < s. \end{cases} \quad (51)$$

Here, ε_w represents the stiffness parameter and s represents the threshold distance. C is the force scale, and \mathbf{x}_s denotes the vector with the smallest norm value which points from one particle to another or points from the wall to the particle. In the lubrication force model, the repulsive force is given as

$$\mathbf{F}_R = \begin{cases} \mathbf{0}, & \text{if } |\mathbf{x}_s| > s, \\ -6\pi\rho\nu \frac{R_a^2 R_b^2}{(R_a + R_b)^2} \left(\frac{1}{|\mathbf{x}_s|} - \frac{1}{s} \right) (\mathbf{v}_a - \mathbf{v}_b) \frac{\mathbf{x}_a - \mathbf{x}_b}{|\mathbf{x}_a - \mathbf{x}_b|}, & \text{if } |\mathbf{x}_s| < s. \end{cases} \quad (52)$$

Here, \mathbf{x}_a and \mathbf{x}_b are the particle center positions, \mathbf{v}_a and \mathbf{v}_b are the corresponding particle velocities along $(\mathbf{x}_b - \mathbf{x}_a)$. Xia et al. [167] and Huang et al. [144] demonstrated that these two repulsive force models give almost the same results.

As a fixed Cartesian grid is used in the LB method, for suspension flow simulation, another issue is to handle the information at “new” fluid nodes, namely the fluid node transformed from the solid node inside a solid particle due to the motion of particles. Recently, Tao et al. [168] examined the spurious force fluctuations produced by various refilling schemes, and they proposed a unified iterative scheme for moving boundaries, which provides a consistent treatment for both boundary nodes and free nodes and can also suppress spurious force fluctuations [169]. Meanwhile, Peng et al. [151] demonstrated the robustness of a velocity-constrained normal extrapolation refilling scheme [170] for particulate flow at high Reynolds numbers.

7 Applications in fuel cells and flow batteries

The application of a gas–liquid two-phase LB model for simulation in a PEMFC gas diffusion layer (GDL) dates back to 2007 by Niu et al. [171] and Sinha et al. [172]. Since then, a variety of studies have been conducted; a condensed review of the work before 2010 can be found by Mukherjee et al. [12]. Here, we would like to add more discussion on this topic in addition to the works that have already been presented in that review paper. For example, Hao and Cheng [173] simulated water invasion in an initially gas filled GDL and investigated the effect of GDL wettability on water transport. They found that in a highly hydrophobic GDL, the water transport exhibits capillary fingering characteristics; in a neutral wettability GDL, water transport falls in the stable displacement regime. Moreover,

saturation in the GDL barely changes after water breaks through it. Their results demonstrated that to alleviate water flooding issues, introducing hydrophilic passages in GDL is a promising strategy. Later, Hao and Cheng [174] simulated two-phase flows in a reconstructed carbon paper GDL (shown in Fig. 7). They calculated the relative permeabilities of body-centered sphere beds at different non-wetting phase saturations and then compared the simulation results with experimental data for further validation. After that, they investigated the wettability effects and the anisotropic characteristics on the relative permeability of GDL. Their results show that the relative permeability of both wetting and non-wetting phases is hardly influenced by the flow orientation, and only the non-wetting phase relative permeability is influenced by the wettability.

Chen et al. [175] investigated the coupled pore-scale fluid flow and mass transport in a carbon paper GDL of a PEMFC with an interdigitated flow channel. The porous geometry is reconstructed based on the statistical information of carbon paper GDL, and the two-phase flow simulation was validated by bubble test and static angle test. They found that in a PEMFC with an interdigitated flow channel, the liquid water within the GDL shows slow creeping characteristics when the capillary force is dominant, and shows quick moving characteristics when the shear force is dominant. What is more, higher contact angle hinders liquid water advancing when the capillary force is dominant, but facilitates liquid water transport when the shear force is dominant.

Efforts have also been made to study gas–liquid two-phase flows in the flow channel of PEMFCs using an LB multiphase model. For example, Hao and Cheng [176] simulated the formation process of a liquid droplet emerging through a pore on the GDL surface, and the subsequent movement of the droplet under gas shear (shown in Fig. 8). They showed the dynamic behavior of the droplet emergence, growth, detachment, and movement in the flow channel. They found that the droplet can be lifted from a highly hydrophobic GDL surface, which facilitates the gas reactant transport as a result of increased GDL surface. It should be noted that droplet dynamics in a channel or on a flat surface have also been extensively studied using the volume of fluid method [177], the level set method [178], and the phase field method [179]. However, these numerical techniques are based on directly solving the Navier–Stokes equations, which remains a challenging issue in simulating multiphase flows, as it is difficult to track the interface dynamics that physically result from microscopic interactions between molecules.

There are also some attempts to apply the coupled fluid flow and mass transport LB model in aqueous redox flow batteries. Qiu et al. [180,181] digitally reconstructed the porous electrode geometries from X-ray computed tomography (XCT) imaging, and the processed XCT data were used as geometry inputs for the pore-scale model to study elec-

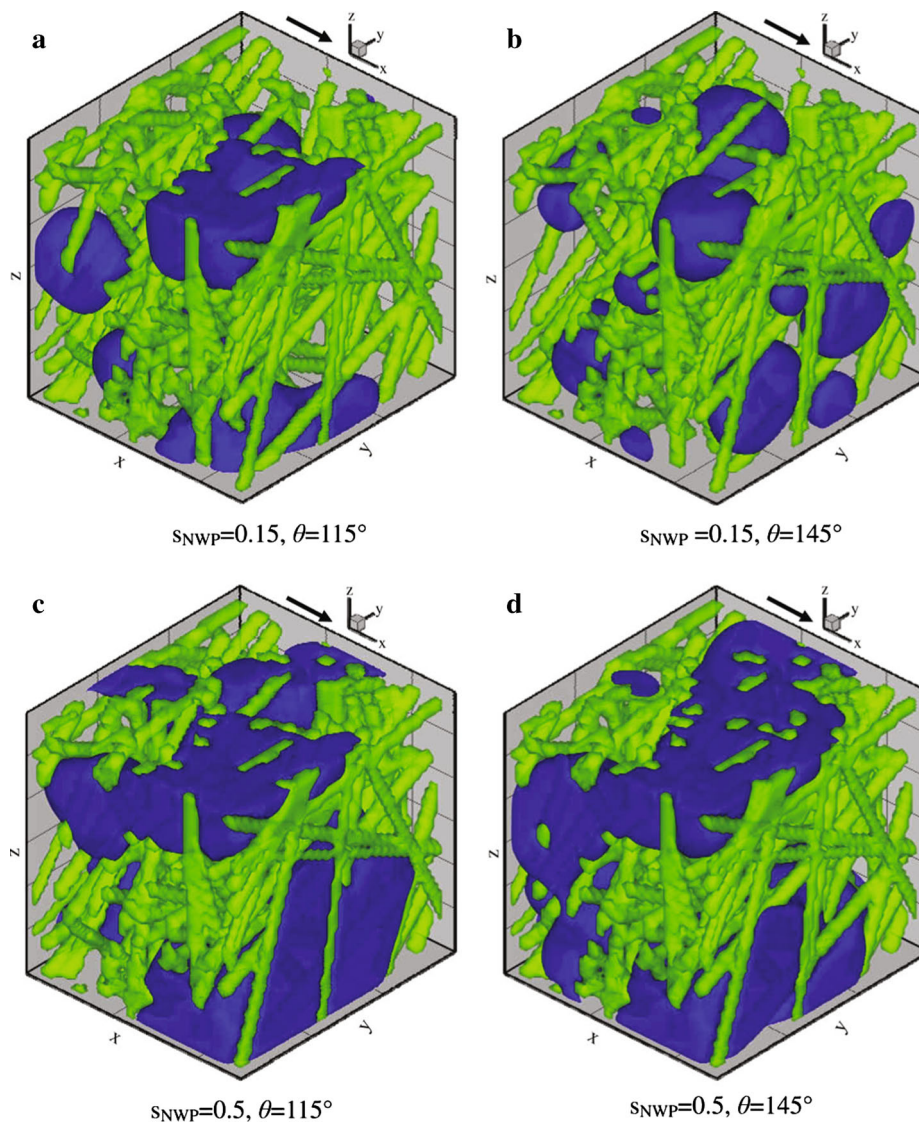


Fig. 7 Non-wetting phase distribution in carbon paper GDL [174]. Reproduced from Ref. [174] (Copyright 2010, Elsevier)

trode morphology effects on the performance characteristics of an all-vanadium redox flow battery. Results were obtained for the pore-scale cell potential distribution, concentration distribution, overpotential and current density distribution (as shown in Fig. 9). They concluded that electrode structures with high surface area and low porosity will result in more uniform and lower overpotential fields, whereas the pressure drop will be increased implying extra consumption of pump work. The influence of electrolyte flow rate and external drawing current on the cell performance has also been investigated. Though the pore-scale simulation results of cell voltage generally agree with a simplified model derived from the charge conservation principle, a more rigorous validation of this model for simulating pore-scale flow field, concentration field, and electron field is a challenge. What is more, the tedious programming implementation and the high cost

of extracting XCT data in this pore-scale approach limits its wide application in the short term.

8 Summary and outlook

The past 30 years have witnessed rapid developments of the LB method in both fundamentals and applications. The potential of the LB method to solve various challenging problems in science and engineering, such as gas–liquid two-phase flows, coupled fluid flow and mass transport in porous media, and particulate flows, has attracted great interest in the computational fluid dynamics and numerical heat transfer communities. This review paper focuses on the above topics and highlights its applications in fuel cells and flow batteries.

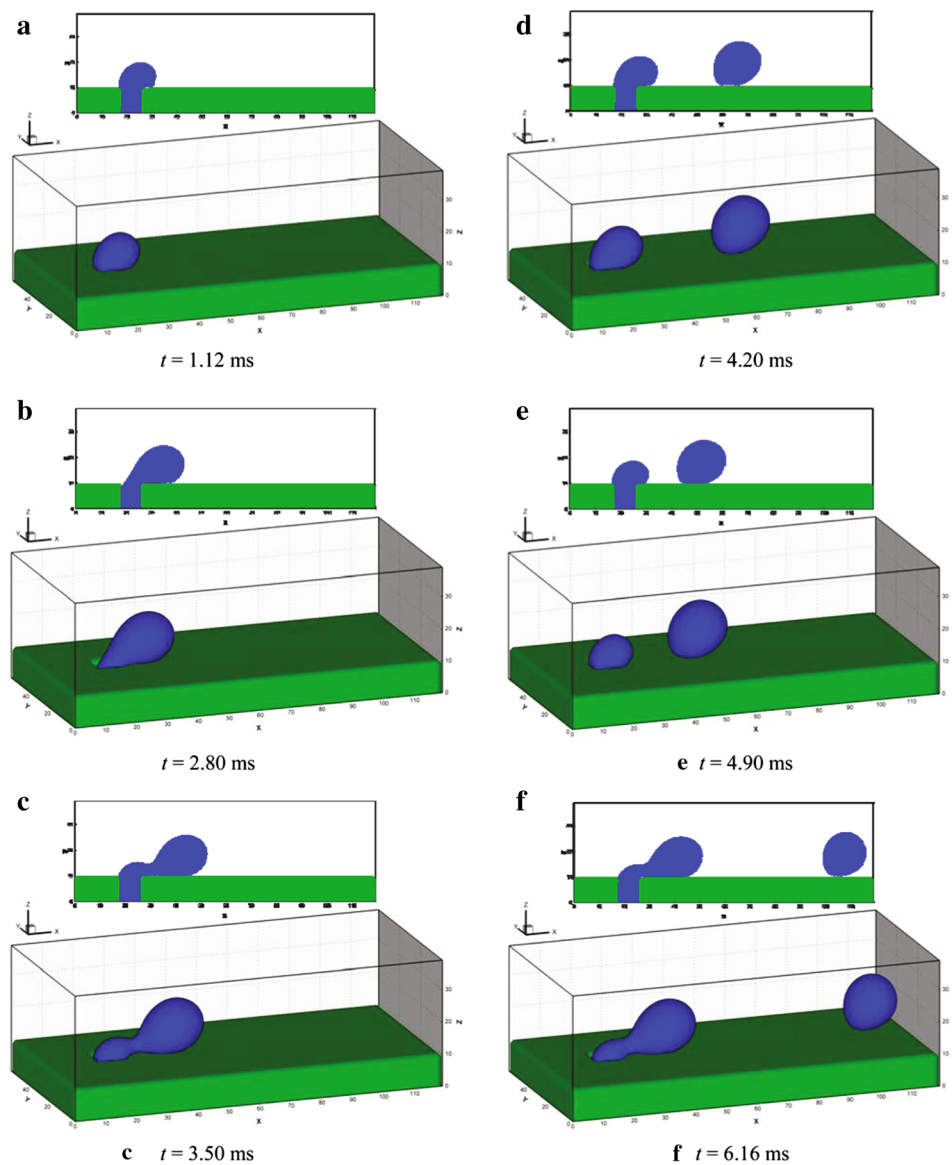


Fig. 8 Snapshots of the droplet formation through a micro-pore in the bottom wall [176]. Reproduced from Ref. [176] (Copyright 2009, Elsevier)

For fuel cell applications, gas–liquid two-phase flows in both the porous media and flow channels of PEMFCs have been extensively explored. However, all the reported simulations are based on isothermal multiphase flow models, while the important thermal effects including evaporation and condensation of water in a PEMFC have not been taken into account. Recent advances in thermal phase change pseudo-potential LB models [79,80] are expected to be applied on this topic in addition to their current applications in flow boiling. A more challenging problem is the simulation of multiphase flows in a DMFC, where the fuels are methanol and oxygen and the products are carbon dioxide gas and water, indicating that multicomponent multiphase flows and coupled phase change heat transfer have occurred [182].

For now, we have not seen theoretical breakthroughs of the LB method for simulating multicomponent multiphase flows with phase change heat transfer.

For aqueous redox flow battery applications, though pioneering work on coupled fluid flow and mass transport in an all-vanadium redox flow battery has been done [180,181], further extension to other aqueous redox flow battery systems is non-trivial. This is mainly due to the fact that electrochemical reactions are strongly coupled with the transport processes in the electrodes of aqueous redox flow batteries, while the correct and efficient implementation of general electrochemical reaction boundary conditions in the LB method deserves further investigation. Another challenging problem using this pore-scale simulation tool is to optimize

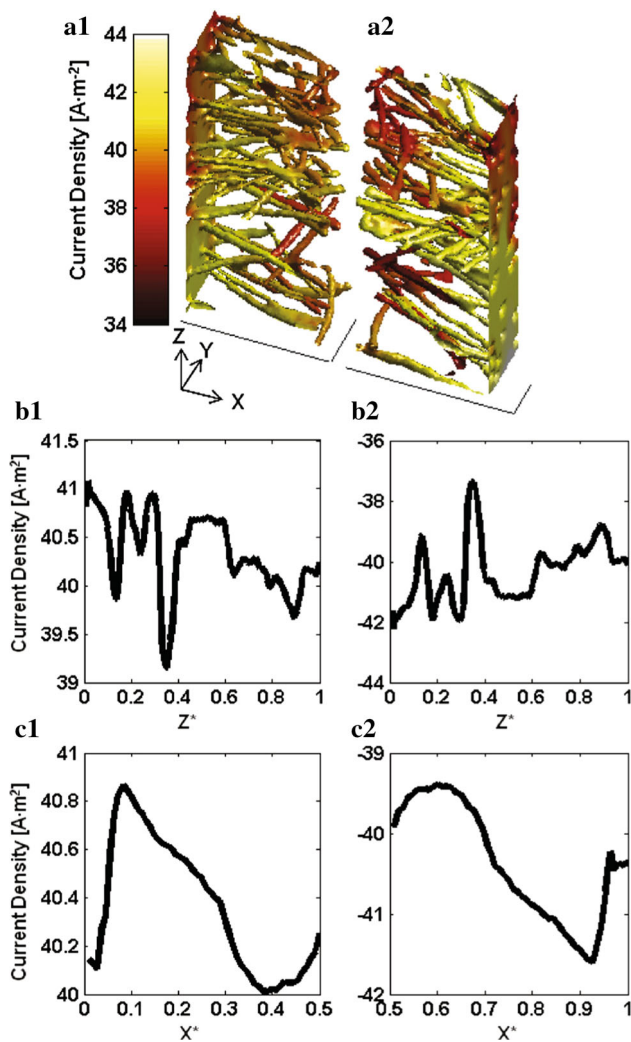


Fig. 9 Pore-scale simulations of current density distribution on the electrode surface [180]. Reproduced from Ref. [180] (Copyright 2012, Elsevier)

the morphology of porous electrodes, including pore size, shape, and distribution, to simultaneously maximize the flow of all the species.

For suspension redox flow battery applications, a key issue is to minimize the viscosity of the suspension fluid while increasing the solid fraction as much as possible. This brings us to the question of modeling dense suspension flows using the LB method, specifically the problem of accurate modeling of the interactions between solid particles. The artificial repulsive force models currently used, such as the spring force model [165] and the lubrication force model [166], can be questioned in their treatment of particle interactions in a dense suspension versus those in a dilute suspension, and the scenarios involving multi-particle collisions make the simulation much more challenging.

In conclusion, the application of the LB method to study transport phenomena in fuel cells and flow batteries is still

not mature enough to support comprehensive technological development. Significant efforts are needed to address both scientific issues and industrial challenges.

Acknowledgements This work was supported by the Research Grants Council of the Hong Kong Special Administrative Region, China (Grant 623313).

References

- Chen, S., Doolen, G.D.: Lattice Boltzmann method for fluid flows. *Annu. Rev. Fluid Mech.* **30**, 329–364 (1998)
- Aidun, C.K., Clausen, J.R.: Lattice-Boltzmann method for complex flows. *Annu. Rev. Fluid Mech.* **42**, 439–472 (2010)
- Guo, Z., Shu, C.: *Lattice Boltzmann Method and Its Applications in Engineering*. World Scientific, Singapore (2013)
- Guo, Z., Zheng, C.: *Theory and Applications of Lattice Boltzmann Method*. Science Press, Beijing (2009)
- He, Y., Wang, Y., Li, Q., et al.: *Lattice Boltzmann Method: Theory and Applications*. Science Press, Beijing (2009)
- He, Y., Li, Q., Wang, Y., et al.: Lattice Boltzmann method and its applications in engineering thermophysics. *Chin. Sci. Bull.* **54**, 4117–4134 (2009)
- Succi, S.: Lattice Boltzmann 2038. *EPL* **109**, 50001 (2015)
- Huang, H., Sukop, M.C., Lu, X.-Y., et al.: *Multiphase Lattice Boltzmann Methods: Theory and Application*. Wiley, New York (2015)
- Li, Q., Luo, K., Kang, Q., et al.: Lattice Boltzmann methods for multiphase flow and phase-change heat transfer. *Prog. Energy Combust. Sci.* **52**, 62–105 (2016)
- Yu, D., Mei, R., Luo, L.-S., et al.: Viscous flow computations with the method of lattice Boltzmann equation. *Prog. Aerospace Sci.* **39**, 329–367 (2003)
- Jiao, K., Li, X.: Water transport in polymer electrolyte membrane fuel cells. *Prog. Energy Combust. Sci.* **37**, 221–291 (2011)
- Mukherjee, P.P., Kang, Q., Wang, C.-Y., et al.: Pore-scale modeling of two-phase transport in polymer electrolyte fuel cells—progress and perspective. *Energy Environ. Sci.* **4**, 346–369 (2011)
- Zhao, T., Xu, C., Chen, R., et al.: Mass transport phenomena in direct methanol fuel cells. *Prog. Energy Combust. Sci.* **35**, 275–292 (2009)
- Xu, Q., Zhao, T.: Fundamental models for flow batteries. *Prog. Energy Combust. Sci.* **49**, 40–58 (2015)
- Yang, Z., Zhang, J., Kintner-Meyer, M.C., et al.: Electrochemical energy storage for green grid. *Chem. Rev.* **111**, 3577–3613 (2011)
- Hatzell, K.B., Boota, M., Gogotsi, Y., et al.: Materials for suspension (semi-solid) electrodes for energy and water technologies. *Chem. Soc. Rev.* **44**, 8664–8687 (2015)
- Wolfram, S.: Statistical mechanics of cellular automata. *Rev. Mod. Phys.* **55**, 601 (1983)
- Frisch, U., Hasslacher, B., Pomeau, Y., et al.: Lattice-gas automata for the Navier–Stokes equation. *Phys. Rev. Lett.* **56**, 1505 (1986)
- McNamara, G.R., Zanetti, G.: Use of the Boltzmann equation to simulate lattice-gas automata. *Phys. Rev. Lett.* **61**, 2332 (1988)
- Qian, Y., D’Humières, D., Lallemand, P., et al.: Lattice BGK models for Navier–Stokes equation. *EPL* **17**, 479–484 (1992)
- He, X., Luo, L.-S.: Theory of the lattice Boltzmann method: from the Boltzmann equation to the lattice Boltzmann equation. *Phys. Rev. E* **56**, 6811 (1997)
- Bhatnagar, P.L., Gross, E., Krook, M.: A model for collision processes in gases. I. Small amplitude processes in charged and neutral one-component systems. *Phys. Rev.* **94**, 511–525 (1954)

23. Xu, K.: Direct Modeling for Computational Fluid Dynamics, vol. 4. World Scientific, Singapore (2015)
24. Xu, K.: Direct modeling for computational fluid dynamics. *Acta Mech. Sin.* **31**, 303–318 (2015)
25. Lallemand, P., Luo, L.-S.: Theory of the lattice Boltzmann method: dispersion, dissipation, isotropy, Galilean invariance, and stability. *Phys. Rev. E* **61**, 6546 (2000)
26. d’Humières, D.: Multiple-relaxation-time lattice Boltzmann models in three dimensions. *Philos. Trans. R. Soc. Lond. Ser. A Math. Phys. Eng. Sci.* **360**, 437–451 (2002)
27. Huang, H., Krafczyk, M., Lu, X., et al.: Forcing term in single-phase and Shan–Chen-type multiphase lattice Boltzmann models. *Phys. Rev. E* **84**, 046710 (2011)
28. Guo, Z., Zheng, C., Shi, B., et al.: Discrete lattice effects on the forcing term in the lattice Boltzmann method. *Phys. Rev. E* **65**, 046308 (2002)
29. Guo, Z., Zheng, C.: Analysis of lattice Boltzmann equation for microscale gas flows: relaxation times, boundary conditions and the Knudsen layer. *Int. J. Comput. Fluid Dyn.* **22**, 465–473 (2008)
30. Tölke, J., Krafczyk, M.: TeraFLOP computing on a desktop PC with GPUs for 3D CFD. *Int. J. Comput. Fluid Dyn.* **22**, 443–456 (2008)
31. Delbosc, N., Summers, J., Khan, A., et al.: Optimized implementation of the lattice Boltzmann method on a graphics processing unit towards real-time fluid simulation. *Comput. Math. Appl.* **67**, 462–475 (2014)
32. Lin, L.-S., Chang, H.-W., Lin, C.-A., et al.: Multi relaxation time lattice Boltzmann simulations of transition in deep 2D lid driven cavity using GPU. *Comput. Fluids* **80**, 381–387 (2013)
33. Chang, H.-W., Hong, P.-Y., Lin, L.-S., et al.: Simulations of flow instability in three dimensional deep cavities with multi relaxation time lattice Boltzmann method on graphic processing units. *Comput. Fluids* **88**, 866–871 (2013)
34. Huang, C., Shi, B., He, N., et al.: Implementation of multi-GPU based lattice Boltzmann method for flow through porous media. *Adv. Appl. Math. Mech.* **7**, 1–12 (2015)
35. Huang, C., Shi, B., Guo, Z., et al.: Multi-GPU based lattice Boltzmann method for hemodynamic simulation in patient-specific cerebral aneurysm. *Commun. Comput. Phys.* **17**, 960–974 (2015)
36. Xu, A., Shi, L., Zhao, T., et al.: Accelerated lattice Boltzmann simulation using GPU and OpenACC with data management. *Int. J. Heat Mass Transf.* **109**, 577–588 (2017)
37. Gunstensen, A.K., Rothman, D.H., Zaleski, S., et al.: Lattice Boltzmann model of immiscible fluids. *Phys. Rev. A* **43**, 4320 (1991)
38. Grunau, D., Chen, S., Eggert, K., et al.: A lattice Boltzmann model for multiphase fluid flows. *Phys. Fluids* **5**, 2557–2562 (1993)
39. Shan, X., Chen, H.: Lattice Boltzmann model for simulating flows with multiple phases and components. *Phys. Rev. E* **47**, 1815 (1993)
40. Shan, X., Chen, H.: Simulation of nonideal gases and liquid-gas phase transitions by the lattice Boltzmann equation. *Phys. Rev. E* **49**, 2941 (1994)
41. Swift, M.R., Osborn, W., Yeomans, J., et al.: Lattice Boltzmann simulation of nonideal fluids. *Phys. Rev. Lett.* **75**, 830 (1995)
42. Swift, M.R., Orlandini, E., Osborn, W., et al.: Lattice boltzmann simulations of liquid-gas and binary fluid systems. *Phys. Rev. E* **54**, 5041 (1996)
43. He, X., Chen, S., Zhang, R., et al.: A lattice Boltzmann scheme for incompressible multiphase flow and its application in simulation of Rayleigh–Taylor instability. *J. Comput. Phys.* **152**, 642–663 (1999)
44. Rothman, D.H., Keller, J.M.: Immiscible cellular-automaton fluids. *J. Stat. Phys.* **52**, 1119–1127 (1988)
45. Huang, H., Huang, J.-J., Lu, X.-Y., et al.: On simulations of high density ratio flows using color-gradient multiphase lattice Boltzmann models. *Int. J. Mod. Phys. C* **24**, 1350021 (2013)
46. Huang, H., Huang, J.-J., Lu, X.-Y., et al.: Study of immiscible displacements in porous media using a color-gradient-based multiphase lattice Boltzmann method. *Comput. Fluids* **93**, 164–172 (2014)
47. Ba, Y., Liu, H., Li, Q., et al.: Multiple-relaxation-time color-gradient lattice Boltzmann model for simulating two-phase flows with high density ratio. *Phys. Rev. E* **94**, 023310 (2016)
48. Yuan, P., Schaefer, L.: Equations of state in a lattice Boltzmann model. *Phys. Fluids* **18**, 042101 (2006)
49. Shan, X.: Analysis and reduction of the spurious current in a class of multiphase lattice Boltzmann models. *Phys. Rev. E* **73**, 047701 (2006)
50. Sbragaglia, M., Benzi, R., Biferale, L., et al.: Generalized lattice Boltzmann method with multirange pseudopotential. *Phys. Rev. E* **75**, 026702 (2007)
51. Kupershtokh, A., Medvedev, D., Karpov, D., et al.: On equations of state in a lattice Boltzmann method. *Comput. Math. Appl.* **58**, 965–974 (2009)
52. Gong, S., Cheng, P.: Numerical investigation of droplet motion and coalescence by an improved lattice Boltzmann model for phase transitions and multiphase flows. *Comput. Fluids* **53**, 93–104 (2012)
53. Li, Q., Luo, K., Li, X., et al.: Forcing scheme in pseudopotential lattice Boltzmann model for multiphase flows. *Phys. Rev. E* **86**, 016709 (2012)
54. Li, Q., Luo, K., Li, X., et al.: Lattice Boltzmann modeling of multiphase flows at large density ratio with an improved pseudopotential model. *Phys. Rev. E* **87**, 053301 (2013)
55. Li, Q., Luo, K.: Achieving tunable surface tension in the pseudopotential lattice Boltzmann modeling of multiphase flows. *Phys. Rev. E* **88**, 053307 (2013)
56. Xu, A., Zhao, T., An, L., et al.: A three-dimensional pseudopotential-based lattice Boltzmann model for multiphase flows with large density ratio and variable surface tension. *Int. J. Heat Fluid Flow* **56**, 261–271 (2015)
57. Li, Q., Zhou, P., Yan, H., et al.: Revised Chapman–Enskog analysis for a class of forcing schemes in the lattice Boltzmann method. *Phys. Rev. E* **94**, 043313 (2016)
58. Reijers, S., Gelderblom, H., Toschi, F., et al.: Axisymmetric multiphase lattice Boltzmann method for generic equations of state. *J. Comput. Sci.* **17**, 309–314 (2016)
59. Inamuro, T., Konishi, N., Ogino, F., et al.: A galilean invariant model of the lattice Boltzmann method for multiphase fluid flows using free-energy approach. *Comput. Phys. Commun.* **129**, 32–45 (2000)
60. Cahn, J.W., Hilliard, J.E.: Free energy of a nonuniform system. I. Interfacial free energy. *J. Chem. Phys.* **28**, 258–267 (1958)
61. Cahn, J.W., Hilliard, J.E.: Free energy of a nonuniform system. III. Nucleation in a two-component incompressible fluid. *J. Chem. Phys.* **31**, 688–699 (1959)
62. Allen, S.M., Cahn, J.W.: Mechanisms of phase transformations within the miscibility gap of Fe-rich Fe–Al alloys. *Acta Metall.* **24**, 425–437 (1976)
63. Wang, H., Chai, Z., Shi, B., et al.: Comparative study of the lattice Boltzmann models for Allen–Cahn and Cahn–Hilliard equations. *Phys. Rev. E* **94**, 033304 (2016)
64. Inamuro, T., Ogata, T., Tajima, S., et al.: A lattice Boltzmann method for incompressible two-phase flows with large density differences. *J. Comput. Phys.* **198**, 628–644 (2004)
65. Lee, T., Lin, C.-L.: A stable discretization of the lattice Boltzmann equation for simulation of incompressible two-phase flows at high density ratio. *J. Comput. Phys.* **206**, 16–47 (2005)

66. Huang, H., Zheng, H., Lu, X.-Y., et al.: An evaluation of a 3D free-energy-based lattice Boltzmann model for multiphase flows with large density ratio. *Int. J. Numer. Methods Fluids* **63**, 1193–1207 (2010)
67. Shao, J., Shu, C., Huang, H., et al.: Free-energy-based lattice Boltzmann model for the simulation of multiphase flows with density contrast. *Phys. Rev. E* **89**, 033309 (2014)
68. Huang, H., Huang, J.-J., Lu, X.-Y., et al.: A mass-conserving axisymmetric multiphase lattice Boltzmann method and its application in simulation of bubble rising. *J. Comput. Phys.* **269**, 386–402 (2014)
69. Liang, H., Chai, Z., Shi, B., et al.: Phase-field-based lattice Boltzmann model for axisymmetric multiphase flows. *Phys. Rev. E* **90**, 063311 (2014)
70. Li, Q., Luo, K., Gao, Y., et al.: Additional interfacial force in lattice Boltzmann models for incompressible multiphase flows. *Phys. Rev. E* **85**, 026704 (2012)
71. Liang, H., Shi, B., Guo, Z., et al.: Phase-field-based multiple-relaxation-time lattice Boltzmann model for incompressible multiphase flows. *Phys. Rev. E* **89**, 053320 (2014)
72. Wang, L., Huang, H.-B., Lu, X.-Y., et al.: Scheme for contact angle and its hysteresis in a multiphase lattice Boltzmann method. *Phys. Rev. E* **87**, 013301 (2013)
73. Huang, J.-J., Huang, H., Wang, X., et al.: Numerical study of drop motion on a surface with stepwise wettability gradient and contact angle hysteresis. *Phys. Fluids* **26**, 062101 (2014)
74. Huang, J.-J., Huang, H., Wang, X., et al.: Wetting boundary conditions in numerical simulation of binary fluids by using phase-field method: some comparative studies and new development. *Int. J. Numer. Methods Fluids* **77**, 123–158 (2015)
75. Liang, H., Shi, B., Chai, Z., et al.: Lattice Boltzmann modeling of three-phase incompressible flows. *Phys. Rev. E* **93**, 013308 (2016)
76. Chao, J., Mei, R., Singh, R., et al.: A filter-based, mass-conserving lattice Boltzmann method for immiscible multiphase flows. *Int. J. Numer. Methods Fluids* **66**, 622–647 (2011)
77. Huang, H., Wang, L., Lu, X.-Y., et al.: Evaluation of three lattice Boltzmann models for multiphase flows in porous media. *Comput. Math. Appl.* **61**, 3606–3617 (2011)
78. Cheng, P., Quan, X., Gong, S., et al.: Chapter four-recent analytical and numerical studies on phase-change heat transfer. *Adv. Heat Transf.* **46**, 187–248 (2014)
79. Gong, S., Cheng, P.: A lattice Boltzmann method for simulation of liquid-vapor phase-change heat transfer. *Int. J. Heat Mass Transf.* **55**, 4923–4927 (2012)
80. Li, Q., Kang, Q., Francois, M., et al.: Lattice Boltzmann modeling of boiling heat transfer: the boiling curve and the effects of wettability. *Int. J. Heat Mass Transf.* **85**, 787–796 (2015)
81. Chai, Z.-H., Zhao, T.-S.: A pseudopotential-based multiple-relaxation-time lattice Boltzmann model for multicomponent/multiphase flows. *Acta Mech. Sin.* **28**, 983–992 (2012)
82. Sukop, M.C., Huang, H., Lin, C.L., et al.: Distribution of multiphase fluids in porous media: comparison between lattice Boltzmann modeling and micro-X-ray tomography. *Phys. Rev. E* **77**, 026710 (2008)
83. Huang, H., Li, Z., Liu, S., et al.: Shan-and-chen-type multiphase lattice Boltzmann study of viscous coupling effects for two-phase flow in porous media. *Int. J. Numer. Methods Fluids* **61**, 341–354 (2009)
84. Huang, H., Lu, X.-Y.: Relative permeabilities and coupling effects in steady-state gas-liquid flow in porous media: a lattice Boltzmann study. *Phys. Fluids* **21**, 092104 (2009)
85. Chen, L., Kang, Q., Mu, Y., et al.: A critical review of the pseudopotential multiphase lattice Boltzmann model: methods and applications. *Int. J. Heat Mass Transf.* **76**, 210–236 (2014)
86. Shan, X.: Pressure tensor calculation in a class of nonideal gas lattice Boltzmann models. *Phys. Rev. E* **77**, 066702 (2008)
87. Li, Q., Luo, K.: Thermodynamic consistency of the pseudopotential lattice Boltzmann model for simulating liquid-vapor flows. *Appl. Therm. Eng.* **72**, 56–61 (2014)
88. Li, Q., Luo, K.: Effect of the forcing term in the pseudopotential lattice Boltzmann modeling of thermal flows. *Phys. Rev. E* **89**, 053022 (2014)
89. Martyts, N.S., Chen, H.: Simulation of multicomponent fluids in complex three-dimensional geometries by the lattice Boltzmann method. *Phys. Rev. E* **53**, 743 (1996)
90. Kang, Q., Zhang, D., Chen, S., et al.: Displacement of a two-dimensional immiscible droplet in a channel. *Phys. Fluids* **14**, 3203–3214 (2002)
91. Benzi, R., Biferale, L., Sbragaglia, M., et al.: Mesoscopic modeling of a two-phase flow in the presence of boundaries: the contact angle. *Phys. Rev. E* **74**, 021509 (2006)
92. Li, Q., Luo, K., Kang, Q., et al.: Contact angles in the pseudopotential lattice Boltzmann modeling of wetting. *Phys. Rev. E* **90**, 053301 (2014)
93. Chai, Z., Zhao, T.: Effect of the forcing term in the multiple-relaxation-time lattice Boltzmann equation on the shear stress or the strain rate tensor. *Phys. Rev. E* **86**, 016705 (2012)
94. Huang, H., Thorne Jr., D.T., Schaap, M.G., et al.: Proposed approximation for contact angles in Shan-and-Chen-type multicomponent multiphase lattice Boltzmann models. *Phys. Rev. E* **76**, 066701 (2007)
95. Gong, S., Cheng, P.: Lattice Boltzmann simulation of periodic bubble nucleation, growth and departure from a heated surface in pool boiling. *Int. J. Heat Mass Transf.* **64**, 122–132 (2013)
96. Gong, S., Cheng, P.: Numerical simulation of pool boiling heat transfer on smooth surfaces with mixed wettability by lattice Boltzmann method. *Int. J. Heat Mass Transf.* **80**, 206–216 (2015)
97. Zhang, C., Cheng, P.: Mesoscale simulations of boiling curves and boiling hysteresis under constant wall temperature and constant heat flux conditions. *Int. J. Heat Mass Transf.* **110**, 319–329 (2017)
98. Li, Q., Kang, Q., Francois, M., et al.: Lattice Boltzmann modeling of self-propelled Leidenfrost droplets on ratchet surfaces. *Soft Matter* **12**, 302–312 (2016)
99. Li, Q., Zhou, P., Yan, H., et al.: Pinning–depinning mechanism of the contact line during evaporation on chemically patterned surfaces: a lattice Boltzmann study. *Langmuir* **32**, 9389–9396 (2016)
100. Lou, Q., Guo, Z., Shi, B., et al.: Evaluation of out flow boundary conditions for two-phase lattice Boltzmann equation. *Phys. Rev. E* **87**, 063301 (2013)
101. Li, L., Jia, X., Liu, Y., et al.: Modified outlet boundary condition schemes for large density ratio lattice Boltzmann models. *J. Heat Transf. Trans. ASME* **139**, 052003 (2017)
102. Nithiarasu, P., Seetharamu, K., Sundararajan, T., et al.: Natural convective heat transfer in a fluid saturated variable porosity medium. *Int. J. Heat Mass Transf.* **40**, 3955–3967 (1997)
103. Guo, Z., Zhao, T.: Lattice Boltzmann model for incompressible flows through porous media. *Phys. Rev. E* **66**, 036304 (2002)
104. Guo, Z., Zhao, T.: A lattice Boltzmann model for convection heat transfer in porous media. *Numer. Heat Transf. B Fundam.* **47**, 157–177 (2005)
105. Liu, Q., He, Y.-L., Li, Q., et al.: A multiple-relaxation-time lattice Boltzmann model for convection heat transfer in porous media. *Int. J. Heat Mass Transf.* **73**, 761–775 (2014)
106. Wang, L., Mi, J., Guo, Z., et al.: A modified lattice Bhatnagar–Gross–Krook model for convection heat transfer in porous media. *Int. J. Heat Mass Transf.* **94**, 269–291 (2016)
107. Rong, F., Guo, Z., Chai, Z., et al.: A lattice Boltzmann model for axisymmetric thermal flows through porous media. *Int. J. Heat Mass Transf.* **53**, 5519–5527 (2010)
108. Chai, Z., Guo, Z., Shi, B., et al.: Study of electro-osmotic flows in microchannels packed with variable porosity media via lattice Boltzmann method. *J. Appl. Phys.* **101**, 104913 (2007)

109. Mattila, K., Puurtinen, T., Hyv aluoma, J., et al.: A prospect for computing in porous materials research: very large fluid flow simulations. *J. Comput. Sci.* **12**, 62–76 (2016)
110. Shi, B., Guo, Z.: Lattice Boltzmann model for nonlinear convection–diffusion equations. *Phys. Rev. E* **79**, 016701 (2009)
111. Li, Q., He, Y., Tang, G., et al.: Lattice Boltzmann model for axisymmetric thermal flows. *Phys. Rev. E* **80**, 037702 (2009)
112. Huang, H.-B., Lu, X.-Y., Sukop, M., et al.: Numerical study of lattice Boltzmann methods for a convection–diffusion equation coupled with Navier–Stokes equations. *J. Phys. A Math. Theor.* **44**, 055001 (2011)
113. Li, Q., Luo, K., He, Y., et al.: Coupling lattice Boltzmann model for simulation of thermal flows on standard lattices. *Phys. Rev. E* **85**, 016710 (2012)
114. Wang, J., Wang, D., Lallemand, P., et al.: Lattice Boltzmann simulations of thermal convective flows in two dimensions. *Comput. Math. Appl.* **65**, 262–286 (2013)
115. Chai, Z., Zhao, T.: Lattice Boltzmann model for the convection–diffusion equation. *Phys. Rev. E* **87**, 063309 (2013)
116. Chai, Z., Zhao, T.: Nonequilibrium scheme for computing the flux of the convection–diffusion equation in the framework of the lattice Boltzmann method. *Phys. Rev. E* **90**, 013305 (2014)
117. Li, Q., Chai, Z., Shi, B., et al.: An efficient lattice Boltzmann model for steady convection–diffusion equation. *J. Sci. Comput.* **61**, 308–326 (2014)
118. Li, Q., Chai, Z., Shi, B., et al.: Lattice Boltzmann model for a class of convection–diffusion equations with variable coefficients. *Comput. Math. Appl.* **70**, 548–561 (2015)
119. Liu, Q., He, Y.-L., Li, D., et al.: Non-orthogonal multiple-relaxation-time lattice Boltzmann method for incompressible thermal flows. *Int. J. Heat Mass Transf.* **102**, 1334–1344 (2016)
120. Guo, Z., Zhao, T., Shi, Y., et al.: A lattice Boltzmann algorithm for electro-osmotic flows in micro fluidic devices. *J. Chem. Phys.* **122**, 144907 (2005)
121. Wang, J., Wang, M., Li, Z., et al.: Lattice Poisson–Boltzmann simulations of electro-osmotic flows in microchannels. *J. Colloid Interface Sci.* **296**, 729–736 (2006)
122. Chai, Z., Shi, B.: Simulation of electro-osmotic flow in microchannel with lattice Boltzmann method. *Phys. Lett. A* **364**, 183–188 (2007)
123. Chai, Z., Shi, B.: A novel lattice Boltzmann model for the Poisson equation. *Appl. Math. Model.* **32**, 2050–2058 (2008)
124. Shi, Y., Zhao, T., Guo, Z., et al.: Simplified model and lattice Boltzmann algorithm for microscale electro-osmotic flows and heat transfer. *Int. J. Heat Mass Transf.* **51**, 586–596 (2008)
125. Tang, G., He, Y., Tao, W., et al.: Numerical analysis of mixing enhancement for micro-electroosmotic flow. *J. Appl. Phys.* **107**, 104906 (2010)
126. Wang, M., Kang, Q.: Modeling electrokinetic flows in microchannels using coupled lattice Boltzmann methods. *J. Comput. Phys.* **229**, 728–744 (2010)
127. Yang, X., Shi, B., Chai, Z., et al.: A coupled lattice Boltzmann method to solve Nernst–Planck model for simulating electro-osmotic flows. *J. Sci. Comput.* **61**, 222–238 (2014)
128. Chai, Z., Shi, B., Guo, Z., et al.: A multiple-relaxation-time lattice Boltzmann model for general nonlinear anisotropic convection–diffusion equations. *J. Sci. Comput.* **69**, 355–390 (2016)
129. Pan, C., Luo, L.-S., Miller, C.T., et al.: An evaluation of lattice Boltzmann schemes for porous medium flow simulation. *Comput. Fluids* **35**, 898–909 (2006)
130. Chai, Z., Shi, B., Lu, J., et al.: Non-Darcy flow in disordered porous media: a lattice Boltzmann study. *Comput. Fluids* **39**, 2069–2077 (2010)
131. Khabbazi, A.E., Ellis, J., Bazylak, A., et al.: Developing a new form of the Kozeny–Carman parameter for structured porous media through lattice-Boltzmann modeling. *Comput. Fluids* **75**, 35–41 (2013)
132. Wang, M., He, J., Yu, J., et al.: Lattice Boltzmann modeling of the effective thermal conductivity for fibrous materials. *Int. J. Therm. Sci.* **46**, 848–855 (2007)
133. Wang, M., Wang, J., Pan, N., et al.: Mesoscopic predictions of the effective thermal conductivity for microscale random porous media. *Phys. Rev. E* **75**, 036702 (2007)
134. Wang, M., Pan, N.: Modeling and prediction of the effective thermal conductivity of random open-cell porous foams. *Int. J. Heat Mass Transf.* **51**, 1325–1331 (2008)
135. Wang, M., Pan, N.: Predictions of effective physical properties of complex multiphase materials. *Mater. Sci. Eng. R Rep.* **63**, 1–30 (2008)
136. Jeong, N., Choi, D.H., Lin, C.-L., et al.: Estimation of thermal and mass diffusivity in a porous medium of complex structure using a lattice Boltzmann method. *Int. J. Heat Mass Transf.* **51**, 3913–3923 (2008)
137. Xuan, Y., Zhao, K., Li, Q., et al.: Investigation on mass diffusion process in porous media based on lattice Boltzmann method. *Heat Mass Transf.* **46**, 1039–1051 (2010)
138. Chai, Z., Huang, C., Shi, B., et al.: A comparative study on the lattice Boltzmann models for predicting effective diffusivity of porous media. *Int. J. Heat Mass Transf.* **98**, 687–696 (2016)
139. van der Hoef, M., van Sint Annaland, M., Deen, N., et al.: Numerical simulation of dense gas-solid fluidized beds: a multiscale modeling strategy. *Annu. Rev. Fluid Mech.* **40**, 47–70 (2008)
140. Tenneti, S., Subramaniam, S.: Particle-resolved direct numerical simulation for gas-solid flow model development. *Annu. Rev. Fluid Mech.* **46**, 199–230 (2014)
141. Qi, D., Luo, L.: Transitions in rotations of a nonspherical particle in a three-dimensional moderate Reynolds number Couette flow. *Phys. Fluids* **14**, 4440–4443 (2002)
142. Qi, D., Luo, L.-S.: Rotational and orientational behaviour of three-dimensional spheroidal particles in Couette flows. *J. Fluid Mech.* **477**, 201–213 (2003)
143. Huang, H., Yang, X., Krafczyk, M., et al.: Rotation of spheroidal particles in Couette flows. *J. Fluid Mech.* **692**, 369–394 (2012)
144. Huang, H., Yang, X., Lu, X.-Y.: Sedimentation of an ellipsoidal particle in narrow tubes. *Phys. Fluids* **26**, 053302 (2014)
145. Yang, X., Huang, H., Lu, X., et al.: Sedimentation of an oblate ellipsoid in narrow tubes. *Phys. Rev. E* **92**, 063009 (2015)
146. Yang, X., Huang, H., Lu, X.: The motion of a neutrally buoyant ellipsoid inside square tube flows. *Adv. Appl. Math. Mech.* **9**, 233–249 (2017)
147. Huang, H., Wu, Y., Lu, X.: Shear viscosity of dilute suspensions of ellipsoidal particles with a lattice Boltzmann method. *Phys. Rev. E* **86**, 046305 (2012)
148. Ladd, A.J.: Numerical simulations of particulate suspensions via a discretized Boltzmann equation. Part 1. Theoretical foundation. *J. Fluid Mech.* **271**, 285–309 (1994)
149. Ladd, A.J.: Numerical simulations of particulate suspensions via a discretized Boltzmann equation. Part 2. Numerical results. *J. Fluid Mech.* **271**, 311–339 (1994)
150. Lishchuk, S., Halliday, I., Care, C., et al.: Shear viscosity of bulk suspensions at low Reynolds number with the three-dimensional lattice Boltzmann method. *Phys. Rev. E* **74**, 017701 (2006)
151. Peng, C., Teng, Y., Hwang, B., et al.: Implementation issues and benchmarking of lattice Boltzmann method for moving rigid particle simulations in a viscous flow. *Comput. Math. Appl.* **72**, 349–374 (2016)
152. Bouzidi, M., Firdaouss, M., Lallemand, P., et al.: Momentum transfer of a Boltzmann-lattice fluid with boundaries. *Phys. Fluids* **13**, 3452–3459 (2001)
153. Lallemand, P., Luo, L.-S.: Lattice Boltzmann method for moving boundaries. *J. Comput. Phys.* **184**, 406–421 (2003)

154. Mei, R., Luo, L.-S., Shyy, W., et al.: An accurate curved boundary treatment in the lattice Boltzmann method. *J. Comput. Phys.* **155**, 307–330 (1999)
155. Mei, R., Shyy, W., Yu, D., et al.: Lattice Boltzmann method for 3-D flows with curved boundary. *J. Comput. Phys.* **161**, 680–699 (2000)
156. Chun, B., Ladd, A.: Interpolated boundary condition for lattice Boltzmann simulations of flows in narrow gaps. *Phys. Rev. E* **75**, 066705 (2007)
157. Tao, S., Guo, Z., Wang, L.-P., et al.: Numerical study on the sedimentation of single and multiple slippery particles in a Newtonian fluid. *Powder Technol.* **315**, 126–138 (2017)
158. Wen, B., Zhang, C., Fang, H., et al.: Hydrodynamic force evaluation by momentum exchange method in lattice Boltzmann simulations. *Entropy* **17**, 8240–8266 (2015)
159. Mei, R., Yu, D., Shyy, W., et al.: Force evaluation in the lattice Boltzmann method involving curved geometry. *Phys. Rev. E* **65**, 041203 (2002)
160. Clausen, J.R., Aidun, C.K.: Galilean invariance in the lattice-Boltzmann method and its effect on the calculation of rheological properties in suspensions. *Int. J. Multiph. Flow* **35**, 307–311 (2009)
161. Chen, Y., Cai, Q., Xia, Z., et al.: Momentum-exchange method in lattice Boltzmann simulations of particle-fluid interactions. *Phys. Rev. E* **88**, 013303 (2013)
162. Wen, B., Zhang, C., Tu, Y., et al.: Galilean invariant fluid-solid interfacial dynamics in lattice Boltzmann simulations. *J. Comput. Phys.* **266**, 161–170 (2014)
163. Xu, A., Zhao, T., Shi, L., et al.: Three-dimensional lattice Boltzmann simulation of suspensions containing both micro- and nanoparticles. *Int. J. Heat Fluid Flow* **62**, 560–567 (2016)
164. Peng, C., Geneva, N., Guo, Z., et al.: Issues associated with Galilean invariance on a moving solid boundary in the lattice Boltzmann method. *Phys. Rev. E* **95**, 013301 (2017)
165. Feng, Z.-G., Michaelides, E.E.: The immersed boundary-lattice Boltzmann method for solving fluid-particles interaction problems. *J. Comput. Phys.* **195**, 602–628 (2004)
166. Ladd, A., Verberg, R.: Lattice-Boltzmann simulations of particle-fluid suspensions. *J. Stat. Phys.* **104**, 1191–1251 (2001)
167. Xia, Z., Connington, K.W., Rapaka, S., et al.: Flow patterns in the sedimentation of an elliptical particle. *J. Fluid Mech.* **625**, 249–272 (2009)
168. Tao, S., Hu, J., Guo, Z., et al.: An investigation on momentum exchange methods and refilling algorithms for lattice Boltzmann simulation of particulate flows. *Comput. Fluids* **133**, 1–14 (2016)
169. Hu, J., Tao, S., Guo, Z., et al.: An efficient unified iterative scheme for moving boundaries in lattice Boltzmann method. *Comput. Fluids* **144**, 34–43 (2017)
170. Wang, L.-P., Peng, C., Guo, Z., et al.: Lattice Boltzmann simulation of particle-laden turbulent channel flow. *Comput. Fluids* **124**, 226–236 (2016)
171. Niu, X.-D., Muneke, T., Hyodo, S.-A., et al.: An investigation of water-gas transport processes in the gas-diffusion-layer of a PEM fuel cell by a multiphase multiple-relaxation-time lattice Boltzmann model. *J. Power Sources* **172**, 542–552 (2007)
172. Sinha, P.K., Mukherjee, P.P., Wang, C.-Y., et al.: Impact of GDL structure and wettability on water management in polymer electrolyte fuel cells. *J. Mater. Chem.* **17**, 3089–3103 (2007)
173. Hao, L., Cheng, P.: Lattice Boltzmann simulations of water transport in gas diffusion layer of a polymer electrolyte membrane fuel cell. *J. Power Sources* **195**, 3870–3881 (2010)
174. Hao, L., Cheng, P.: Pore-scale simulations on relative permeabilities of porous media by lattice Boltzmann method. *Int. J. Heat Mass Transf.* **53**, 1908–1913 (2010)
175. Chen, L., Luan, H.-B., He, Y.-L., et al.: Pore-scale flow and mass transport in gas diffusion layer of proton exchange membrane fuel cell with interdigitated flow fields. *Int. J. Therm. Sci.* **51**, 132–144 (2012)
176. Hao, L., Cheng, P.: Lattice Boltzmann simulations of liquid droplet dynamic behavior on a hydrophobic surface of a gas flow channel. *J. Power Sources* **190**, 435–446 (2009)
177. Hirt, C., Nichols, B.: Volume of fluid (VOF) method for the dynamics of free boundaries. *J. Comput. Phys.* **39**, 201–225 (1981)
178. Sethian, J., Smereka, P.: Level set methods for fluid interfaces. *Annu. Rev. Fluid Mech.* **35**, 341–372 (2003)
179. Badalassi, V., Cenicer, H., Banerjee, S., et al.: Computation of multiphase systems with phase field models. *J. Comput. Phys.* **190**, 371–397 (2003)
180. Qiu, G., Joshi, A.S., Dennison, C., et al.: 3-D pore-scale resolved model for coupled species/charge/fluid transport in a vanadium redox flow battery. *Electrochim. Acta* **64**, 46–64 (2012)
181. Qiu, G., Dennison, C., Knehr, K., et al.: Pore-scale analysis of effects of electrode morphology and electrolyte flow conditions on performance of vanadium redox flow batteries. *J. Power Sources* **219**, 223–234 (2012)
182. Chen, R., Zhao, T., Yang, W., et al.: Two-dimensional two-phase thermal model for passive direct methanol fuel cells. *J. Power Sources* **175**, 276–287 (2008)